Analyse the Effect of Filler Material on the TIG Welded AA6082 Aluminium Alloy

A DISSERTATION

SUBMITTED IN PARTIAL FULFILLMENT OF THE REQUIREMENTS FOR THE AWARD OF THE DEGREE

OF

MASTER OF TECHNOLOGY

IN

PRODUCTION AND INDUSTRIAL ENGINEERING

Submitted by

Shivam Sharma

2K20/PIE/07

Under the supervision of

Dr. Vipin

Professor

(Mechanical Engineering Department)

DEPARTMENT OF MECHANICAL ENGINEERING

DELHI TECHNOLOGICAL UNIVERSITY

(Formerly Delhi College of Engineering)

Bawana Road, Delhi-110042

MAY, 2022

CANDIDATE'S DECLARATION

I, **Shivam Sharma** , Roll No. **2K20/PIE/07** of M.Tech (Production and Industrial Engineering), hereby certify that the project Dissertation titled "**Analyse the effect of filler material on the TIG welded AA6082 Aluminium Alloy** " which is submitted by me to the Department of Mechanical Engineering, Delhi Technological University, Delhi in partial fulfilment of the requirement for the award of the degree of the Master of Technology, is original and not copied from any source without proper citation. This work has not previously formed the basis for the award of any Degree, Diploma Associateship, Fellowship or other similar title or recognition.

Place: Delhi

Date:

Shivam Sharma

2K20/PIE/07

M.Tech (Production Engineering)

Delhi Technological University

CERTIFICATE

I hereby certify that the Project Dissertation titled **"Analyse the effect of filler material on the TIG welded AA6082 Aluminium Alloy"** which is submitted by **SHIVAM SHARMA**, 2K20/PIE/07, Mechanical Engineering Department, Delhi Technological University, Delhi in partial fulfilment of the requirement for the award of the degree of Master of Technology, is a record project work carried out by the student under my supervision. To the best of my knowledge this work has not been submitted in part or full for any Degree or Diploma to this University or elsewhere.

Place: Delhi

Date:

Dr. Vipin

SUPERVISOR

Professor

Department of Mechanical Engineering

Delhi Technological University

ACKNOWLEDGEMENT

First of all, I wish to convey my deep gratitude and sincere thanks to my M. Tech supervisor, Dr Vipin for giving me an opportunity to pursue this research work at Delhi Technological University. I feel very fortunate that I got an opportunity to work under his supervision. I would like that thank all the staff and faculty members of Mechanical Engineering Department for their continuous help, encouragement and support.

SHIVAM SHARMA

2K20/PIE/07

MTech (Production Engineering)

Delhi Technological University

ABSTRACT

Aluminium alloys are widely used in industries like construction, automobile, spacecraft manufacturing due to its outstanding properties like high resistance to corrosion, high strength to weight ratio, machinability and ductility. This research aims to analyse the effect of filler material and finding suitable filler wire to weld similar AA6082 Aluminium alloy using GTAW process. A butt joint of similar AA6082 Aluminium Alloy has been produced using 3 different fillers e.g.: ER5356(Mg-rich), ER4043(Si-rich) and ER4047 (Si-rich) at different level of process parameters e.g.: Welding electric current, Diameter of filler wire and gas flow rate of shielding gas. Welding was done in single pass with argon as a shielding gas. Taguchi L9 orthogonal array technique for weld specimen with each filler wire was employed to perform the experiments to investigate the tensile strength. The size of samples was prepared as per the ASME Standard. Hardness test, Residual stress test and microstructure analysis of the optimized weld joints were also investigated. The results revealed that weld specimen with ER 5356 yields more tensile strength, hardness value and low residual stress in comparison to its counterpart's weld specimen with ER4043 and ER4047. Microstructure analysis of all weld specimens reveals that weld zone consist of homogeneous distribution of silicon and aluminium. Better results were obtained with ER5356 as compared to ER4043 and ER4047.

Keywords: AA6082, ER4043, ER4047, ER5356, TIG, Taguchi technique, Tensile Test, Microhardness, Residual stress, Microstructure.

TABLE OF CONTENTS

LIST OF FIGURES

LIST OF TABLES

CHAPTER 1

INTRODUCTION

In modern industrial applications like automobile manufacturing, aircraft construction and shipbuilding, Aluminium alloys are explored to obtain a cost favorable weight optimized body which provide high strength and stiffness. Whereas aluminum has some remarkable characteristics as a pure element, it may not be strong enough for the intent of high durability. As a result, it can be mixed with other elements to form alloys that are much more robust and better suited for industrial uses. An "alloy" is a combination of different metallic elements that is often created to improve the material's strength and durability. Depending on the application and Aluminium alloys usually composed of the pure aluminum combined with other elements like silicon, manganese, tin, copper and magnesium. Aluminum can probably gain more strength with the right mixture, and in some cases, it can even outmatch steel. Alloys offer a similar benefit as pure Aluminium while being less expensive.

1.1 APPLICATIONS OF ALUMINIUM ALLOY

1.1.1 Aerospace sector:

Aerospace industry heavily rely on Aluminium because of three excellent properties of it, which are outstanding ductility, high corrosion resistance and superior strength to weight ratio. As strength of aluminum is comparable to steel with fraction of weight, it provides better fuel efficiency and allow aircrafts to carry more weight for cargos and passengers. Excellent corrosion resistance characteristic of aluminum alloy aids in ensuring safety of aircraft and passengers.

1.1.2 Shipbuilding Construction:

Aluminium is widely used in construction of ships, steel boats and underwater vessels because lightweight property of Aluminium allow more surface and less mass without sacrificing strength which is required to resist cracks in the hull

1.1.3 Automobile sector:

Aluminum is becoming the "preferred material" for car manufacturers, because Aluminium is marketed as being the most cost-effective and environmentally friendly material available for improving performance and diminishing emissions. By employing Aluminium it will be easy to manufacture light weight vehicles without sacrificing strength and durability

1.1.4 Building and construction:

Building materials made of high-strength Aluminium alloy are also extremely popular. Steel is still one of the most important construction materials, while Aluminium alloys are apparently a good runner. It is critical to account for strength and safety when constructing advanced

buildings and structures. Aluminum's inherent insulating feature, as well as its great corrosion resistance and low flammability, making it an excellent option. Aluminum has recently received high international ratings for use in structures where a fire outbreak is a probability. When compared to a same quantity of steel, it takes nearly twice as much heat to raise the temperature of Aluminium by one degree.

1.1.5 Electronics Equipment:

Aluminium is rapidly used in the manufacturing of Mobiles, tablets, laptops, Television, desktop monitors, and other devices. Aluminium is both beautiful and functional, with the capacity to look classy while remaining dependable. These are critical characteristics in the electronics sector. Aluminium contributed to a surge in its use among electronics items manufacturers because it is stronger and much more dependable than plastic while being lighter than steel, which, coupled with its inherent capacity to absorb and distribute heat.

1.2 TYPES OF ALUMINIUM

Aluminium alloy can be divided into two major categories which are Cast Aluminium alloys and wrought Aluminium alloys. Cast Aluminium alloys have more than 22% alloying elements by composition, whereas wrought Aluminium alloys contain less than 4%. The proportion of alloying elements has a significant influence on mechanical properties. When more alloying elements are introduced, Aluminium lacks its ductility, rendering most cast alloys vulnerable to brittle fracture. Wrought alloys, on the other hand, have permit researchers to increase the strength, resistance to corrosion, conductivity, and other properties of Aluminium while maintaining ductility and other desirable properties.
The preponderance of Aluminium goods, such as those made by extrusion or rolling, are made of wrought Aluminium. Individual wrought Aluminium alloy classifications are defined by elements such as copper, manganese, silicon, magnesium, magnesium silicon combinations, zinc, and lithium.

Wrought Aluminium Grades:

A four-digit marker is being used to name wrought Aluminium alloys, where primary alloying elements are represented by the first digit. The second digit represents the initial alloy variation. Individual alloy variation is represented by the third and fourth digits.
Following list shows all grades of wrought Aluminium alloy:

a. **1xxx series:**
   These alloys are 99% pure Aluminium. They are soft and ductile having outstanding corrosion resistance property and formability. They are outstanding chemical and electrical materials. They can be welded by any method, but cannot be heat treated.1xxx series widely used in chemical and food processing industries.

b. **2xxx series:**
   These alloys mostly contain copper and, in some cases, modest amounts of magnesium. With its combination of high strength and remarkable fatigue resistance, it is typically

employed where a good strength-to-weight ratio is necessary. This grade has low resistance to corrosion. Once heat-treated, they achieve excellent strength, rivalling low carbon steels, although they are vulnerable to rust due to their copper content.

c. 3xxx series:

Manganese is the principal alloying ingredient of 3xxx alloys, which enhances their strength over non-heat treatable alloys like the 1xxx family. They're medium-strength alloys with excellent working and finishing properties.3003 Aluminium of this series is most widely used Aluminium alloy is composed of pure Aluminium and manganese which increase its strength. Welding and deep drawing can be performed on this series.

d. 4xxx series:

Silicon is used as an alloying element in 4xxx alloys. Addition of silicon lowers the melting point without sacrificing the ductility. They're widely used to join different grades of Aluminium as welding wire and brazing alloy. Generally, this series of alloys are not heat treatable. 4xxx alloys have attractive oxide coatings that are frequently used in architectural applications.

e. 5xxx series:

Magnesium is the most common alloying ingredient in 5xxx alloys, with minute amounts of manganese in some alloys. 5xxx alloys are commonly used in boat hulls, gangplanks, and other marine equipment. These alloys are strain-hard enabling, weldable, and have excellent corrosion resistance, particularly in marine conditions.

f. 6xxx series:

Magnesium and silicon are the primary alloying components of 6xxx alloys. They have a good balance of strength, ductility, weldability, machinability, and corrosion resistance. Heat treatment improves their strength but still they are not as strong as 2xxx and 7xxx alloys. Architectural, marine, and general-purpose applications are all common uses for them.

g. 7xxx series:

Zinc is used as the principal alloying ingredient in these series of alloys and makes them strongest of all wrought alloys, with strengths exceeding some steels. The presence of zinc reduces workability and machinability, but its high strength compensates for these drawbacks. Because it is one of the highest strengths Aluminium alloys available, it is ideal for aircraft applications, mobile equipment, and other highly stressed parts.

h. 8xxx series:

8xxx alloys are made up of a variety of alloying elements and are used for a variety of purposes, including high-temperature performance, reduced densities, increased stiffness, and other special features. They're typically found in helicopter parts and other space applications.

1.3 WELDING OF ALUMINIUM

Welding is a process of producing localized permanent joint with or without application of heat with or without application of pressure or pressure alone and with or without application of filler material for joining of similar or dissimilar material
Aluminium welding differs from welding steel or iron. Because of the peculiar composition of Aluminium, users might anticipate to face a number of difficulties, these problems are Hot cracking, Porosity and thermal conductivity.
Aluminium can be welded by following processes:

- **a.** Gas Tungsten arc welding (GTAW)
- **b.** Gas Metal arc welding (GMAW)
- **c.** Resistance welding
- **d.** Laser beam welding
- **e.** Electron beam welding

1.3.1 Gas tungsten arc welding (GTAW):

GTAW is an arc welding process arc is generated between non-consumable tungsten electrode and workpiece to produce the weldment. Liquid metal in the weld pool can be protected from oxidation by providing inert gases (helium and argon). Although some welds, known as autogenously welds, do not require a filler metal, it is usually employed. When conducted by trained operators, gas tungsten arc welding can yield greater welded joints because it allows more command over the weld zone than some other welding methods. Weld quality improves dramatically when sterility is maintained. Oil, moisture, filth, and other contaminants must be removed from all equipment and supplies.

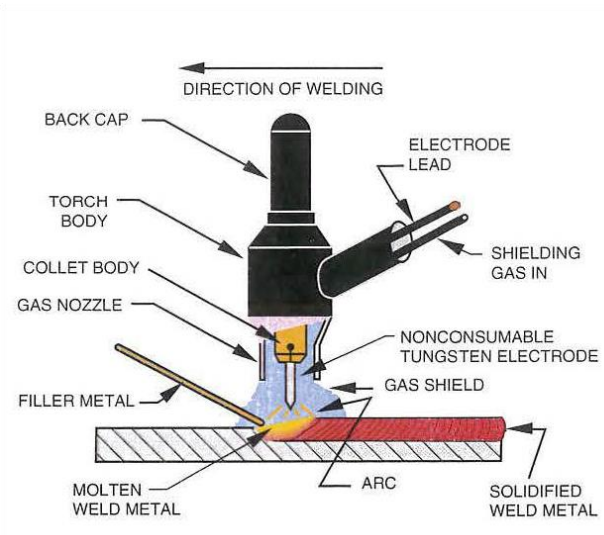

Figure 1.1: Schematic diagram of GTAW

1.3.2 Gas metal arc welding (GMAW):

GMAW is a welding process in which an electric arc is generated between a consumable wire electrode and the work piece metal and the wire will be supplied to the workpiece through the movement of rollers. Roller movement can be controlled by using servomechanism. The material is heated by the electric arc, which induces melting and joining. A shielding gas (Helium, Argon or Carbon dioxide) is fed through the welding gun together with the wire electrode, sheltering the operation from impurities in the air. AC or DCRP power supply with high rate of current is used for welding of aluminium and magnesium alloys. Metal can be transferred from Electron to workpiece in the form of spray transfer due to this depth of penetration is maximum in this welding technique.

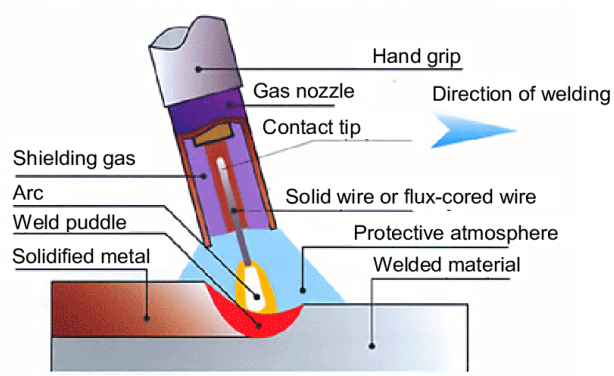

Figure 1.2: Schematic diagram of GMAW

1.3.3 Resistance spot welding (RSW):

RSW is a method of joining of sheet material in mass production. Two sheets are provided between two copper electrodes, by supplying high rate of current for small fraction of time heat will be generated at the contact of two surfaces, after getting sufficient amount of heat by applying pressure joint can be found between two surfaces below the electrode. Leak proof joint is not possible in this process.

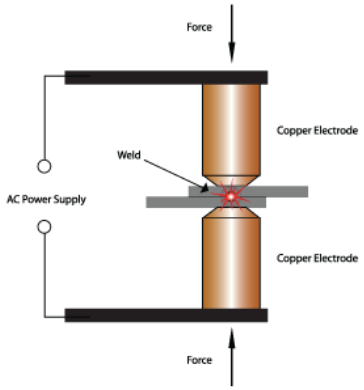

Figure 1.3: Schematic diagram of RSW

1.3.4 Laser beam welding (LBW):

LBW is a laser-based welding technology for joining metal or polymer parts. The beam provides a focused heat source, facilitating for thin, deep welds and fast welding speeds. [2]. The method is often employed in automated high-volume operations, such as the automobile industry.

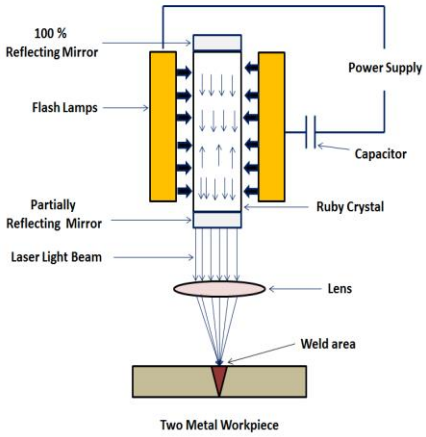

Figure 1.4: Schematic diagram of LBW

1.3.5 Cold Metal Transfer (CMT):

The fundamental feature of this method is an extremely steady arc with very little heat input. The MT welding method allows users to attain optimal settings while combining various materials, during welding when a short circuit is detected, the digital process control detaches the droplet by retracting the wire, as soon as a short circuit develops, the wire travels forward and is pulled back. As a consequence, during the arc-burning phase, the arc only generates heat for a relatively brief time. The arc length is detected and calibrated mechanically. In this process, no matter how rapidly the operator welds or how rough the work piece's surface is, the arc remains stable. The above discussion leads to the conclusion that CMT is highly useful for welding everywhere.

CHAPTER 2

LITERATURE REVIEW

Aluminium alloys are becoming increasingly popular among the manufacturing and fabrication industry because of their flexibility, reliability and strength, but at the same Aluminium alloys present many problems during welding including high thermal conductivity, oxide formation at surface and hydrogen solubility. To overcome these problems various researchers performed numerous researches on welding of Aluminium alloys, which are following:

Lutjanid [1] investigated the most serious complications in welding aluminium alloy is the occurrence of porosity of hydrogen gas in the course of solidification of weld, reason of this is difference in hydrogen solubility between solid and liquid aluminium alloy. Porosity of hydrogen gas comes into existence when dissolved hydrogen is not allowed to escape during solidification.

Missori & Sili [2] analyse the results of test of mechanical properties of AA6082 and found that tensile resistance is directly proportionate to the welding speed. Softening of the material in the Weld bead and heat affected area was also observed at an entity lower than the melting weld.

Ambriz et al. [3] carried out GTAW welding on 12.7 mm thick plate of AA6061 and measure the tensile and hardness properties of welded samples to generate a relationship between these two properties. Hardness was deemed to be a reliable method estimating yield and tensile strength of the heat affected area.

Y. Lakshminarayanan et al. [4] conduct GMAW and GTAW on AA6061 alloy of 6mm thickness to find the influence of welding parameters on tensile properties of aluminium joint. The results demonstrated that the mechanical properties of weld were highly dependent on welding conditions and parameters. Tensile strength and hardness value of welded joint comes out to be more when GTAW technique was used.

Wang et al. [5] investigated effects of TIG arc welding process parameters on microstructure, tensile strength and fracture of Ni base welded joint. Welding current of ranging between 50A to 90A, with changing speed in the range of 2100mm/min to 2900mm/min was used for welding of plate with width 1.2mm to 1.5mm.

Norma et al. [6] investigated the microstructure of Al-Mg-Cu-Mn alloy welded by GTAW for a broad range of welding conditions. Range of welding current was 100A to 190A and range of welding speed was 420mm/min to 1500mm/min. He reported that in comparison to the fusion boundary, weld centre cools at faster rate due to which fine microstructures noted at the centre of weld. It was also reported that on increasing welding current, cooling rate also increases at the centre of weld, which results in formation of small dendrite structure.

Urena et. al. [7] The fracture behaviour of TIG welded Al matrix composites was examined in relation to the interfacial response between the Al alloy (2014) matrix and SiC particle reinforcement. On 4 mm thick AA2014/SiC/Xp sheets, TIG welding was performed with a current setting of 37-155 A and a voltage of 14-16.7 V. The failure occurred in the weld metal with a tensile strength less than 50% of the parent material, according to experimental results. Interface deboning via the interface reaction Layer was used to regulate welded joint fracture. The creation of Aluminium-carbide lowers the matrix/reinforcement interface strength, increasing the risk of interfacial failure in the weld zone.

Kumar & Sundarrajan [8] Performed Pulsed TIG welding of 2.14 mm AA5456 Al alloy with a welding current of 40-90 A and a welding speed of 210-230 mm/min. To improve the mechanical properties of pulsed TIG welding, the Taguchi method was used to optimise the process parameters and regression models were created. All of the welds' microstructures were examined and correlated with their mechanical properties. Planishing resulted in a 10-15% improvement in mechanical characteristics due to the dispersion of internal stresses in the weld.

Durgutlu [9] explored the effect of hydrogen in argon as a shielding gas for TIG welding of austenitic stainless steel 316L was explored. For welding a 4 mm thick plate, they employed 115 A current, 100 mm/min welding speed, and 10 l/min gas flow rate. Weld metal has a lower hardness than HAZ and base metal for all shielding medium. With increasing hydrogen content, penetration depth, weld bead width, and mean grain size in the weld metal rise. The sample welded under a shielding gas of 1.5 percent H2–Ar had the maximum tensile strength.

Hussain et. al. [10] carried out TIG welding of AA6351 Aluminium alloy with a thickness of 4 mm was used to evaluate the influence of welding speed on the tensile strength of the welded connection. A universal tensile testing machine was used to determine the strength of the welded junction. Single v butt joint specimens were welded at speeds ranging from 1800 to 7200 mm/minute. Experimental results demonstrated the weld zone has a lower strength than the base metal and that tensile strength increases as welding speed is reduced.

Qinglei et. al. [11] investigated the microstructure, element distribution, phase components, and micro hardness of a TIG welding joint of Mo-Cu composite and 18-8 stainless steel plates with a thickness of 2.5 mm. Welding was carried out at a speed of 49.8-64.2 mm/min, with a gas flow rate of 8 l/min, an arc voltage of 28-32%, and a welding current of 90 A. The high micro hardness must be due to the formation of -Fe (Ni) phases and the Fe0.54Mo0.73 combination. The results show that the weld metal contains austenite and ferrite phases. The micro hardness near the fusion zone on the Mo–Cu composite side increased from weld metal to fusion zone, with a peak around the fusion zone/Mo–Cu composite boundary.

Sanjeev [12] employed TIG welding to investigate the feasibility of welding thicker plates. Pulsed Tungsten Inert Gas Welding was used to weld aluminium plates (3-5mm thickness) with a welding current of 48-112 A and a gas flow rate of 7-15 lt./min. Weld metal has a lower shear strength (73MPa) than parent metal (85 MPa). Weld deposits create co-axial dendritic micro-structure towards the fusion line, and tensile fracture occurs near the fusion line of weld deposit, according to photomicrographs of welded specimens.

Indira Rani et. al. [13] conduct GTAW/TIG welding with non-pulsed and pulsed current at various frequencies to explore the mechanical properties of welded joint of AA6351 alloy. Welding was done at 70-74 A current, 700-760 mm/min arc travel speed, and 3 and 7 Hz pulse frequency. Based on the experimental results, it was determined that the weldments' tensile strength and yield strength are closer to base metal. Weldment failure occurred at HAZ, and as a result, we concluded that weldments have higher weld joint strength.

Ghazvinloo et al. [14] carried out MIG robotic welding on AA6061 to explore the effect of parameters like arc voltage, welding speed and welding electric current on fatigue life and impact energy of AA6061 welded joint. Various samples were prepared using arc voltages of 20V, 23V, and 26V. Welding currents of 110A,130A,150A and welding speed of 50,60 and 70cm/min. Results shows that when heat input is increased, fatigue life of weld metal diminishes, whereas impact energy of weld metal increases initially and then decreases significantly.

Mosneaga et al. [15] is being carried out to assess the level of mechanical properties, particularly impact toughness, of welded Al-Mg-Si alloys with varying amounts of Mn addition and using two types of fillers, Al-Si (A4043) and Al-Mg (A5356). Effect of microstructure on toughness is given special consideration. The effects received display dead the toughness of welded metal maybe progressed 20-30% with the aid of including Mn. Using AA4043 filler wire, extent of absorbed energy decreases as Mg content rises, and low Mg and no Mn addition results in a good combination of mechanical properties. The level of absorbed energy, however, increases as the Mg content increases and decreases as the Si content increases when using the A5356 filler. Alloy had the highest value of absorbed energy in this case (0.7 percent Mn). The toughness of A5356 filler is approximately 56% greater than that of A4043 filler.

Dongjie Li et.al. [16] carried out double shielded GTAW welding to increase depth of penetration, a double-shielded TIG welding model was introduced and matched to the standard TIG welding method using different welding factors such as welding speed, arc length, and current. They employed a 10 lt/min gas flow rate with a welding speed of 400 rpm,(90-300) mm/min, current (100-200) A, and w/p 10 mm thickness the findings reveal that he oxygen content in the weld is directly affected by changes in welding parameters.

Karunakaran [17] carried out TIG welding of AISI 304L stainless steel, and the weld bead profiles for constant and pulsed current settings were compared. The effect of welding current on the tensile strength, hardness profiles, microstructure, and residual stress distribution of steel samples was investigated. Welding currents of 100-180 A, welding speed of 118.44 mm/min, and pulse frequency of 6 Hz were used in the experiments. In comparison to continuous current welding, pulsed current welding produced lower internal stresses. Use of such pulsed current improved the tensile and hardness properties of the joints by forming finer grains and breaking dendrites.

Juang [18] performed TIG welding of stainless steels to get best process parameters for appropriate weld pool Geometry. Taguchi technique was employed to find the effect of parameters on the geometry of weld pool.

Shahi et. al. [19] analyse the different variables of welding process which effect the tensile strength of butt welded joint produced by submerged arc welding. Results reveals that welding electric current was the most important factor regards to UTS and hardness of welded joint.

L. Kwang Pan et. al. [20] illustrate that The Taguchi approach is an effective tool for creating greater systems. It gives a methodical process to enhancing designs for productivity and effectiveness, rather than just an efficient technique The Taguchi experimental strategy can enhance efficiency by adjusting design parameters and reducing overall system internal and external factors to covariate.

Senthil Kumar et al. [21] used pulsed current tungsten inert gas welding to join AA6061 aluminium alloy and tuned the settings to achieve maximum tensile strength of the joints

Sanja [22] performed the GTAW welding of thin aluminium sheets with Helium and helium and argon mixture as shielded gas. Results illustrates that better weld geometry produces with the mixture of helium and argon as a shielded gas.

Qiang Zhu et. al. [23] Researchers investigated that weldability of 6000 series is better than 7000 series of Aluminium and TIG welding is better suitable for welding Aluminium Alloys when considering welding equipment, processing costs, and manufacturing technology

G. Satish Kumar et. al. [24] carried out GTAW welding of Aluminium AA6082 alloy with 5356 filler wire at different level of various process factors like welding electric current, flow rate of shielded gas and travel speed of welding torch. Optimum values of process parameters have been found by employing grey relational technique. Investigation results revealed that strength of weld joint increases with increase in electric current and hardness of joint decreases with increase in electric current.

2.1 RESEARCH GAP

On the basis of literature Review the following research gap have been identified:

- Although GTAW is one of the efficient process for welding of Aluminium, but it is a significant challenge to weld the Aluminium defect free.
- Small amount of efforts has been made on TIG welding AA 6082 using the filler materials 4043,4047 and 5356.
- Ideas to improve wettability in molten pool by employing different filler material has not been studied much.
- Use of different filler materials and its effect with varying welding parameters is also found to be missing.

2.2 OBJECTIVES OF WORK

Aluminium has a wide spectrum of uses in practically all industrial zones because they provide a greater strength-to-weight ratio. As a result, there is a need to concentrate on the welding issues with these materials so that they may be used more efficiently. We've seen a lot of research gaps in the subject of welding AA6082 metals, thus the study's main goal is to look an employing different filler material in welding of AA6082 to improve the quality of weld.

- To form a sound weld joint using GTAW process with ER4043, ER4047and ER5356 filler wire.
- Optimization of different welding parameters for good welding quality with each filler wire.
- Characterization of welded joint with each filler wire and to find out the effect of each filler wire on the welded joint of AA6082 alloy.

CHAPTER 3

EXPERIMENTAL WORK AND METHODOLGY

3.1 MATERIAL SELECTION

3.1.1 Aluminium AA6082:

AA6082 Aluminium alloy has highest strength among all the 6000 series. It is also called as Structural alloy. Silicon and manganese are main constituents of AA6082. It is well-known for its machining capabilities, but it also has outstanding weldability, cold machinability, and resistance to corrosion. It is well-known for its machining capabilities, but it also has outstanding weldability, cold machinability, and resistance to corrosion. Because of its high manganese content, it is able to manage its grain structure, leading to a stronger alloy that is ideal for applications requiring extra strength and toughness.

3.1.2 ER4043:

Filler rod ER4043 is a general-purpose kind. It is one of the most extensively used welding and brazing alloys. Silicon as the main constituent of this alloy improves the weld pool's wetting action and make the weld less prone to cracking. ER4043 is used to weld a variety of Aluminium grades.

3.1.3 ER5356:

Filler rod ER5356 is a Magnesium rich alloy, which is usually chosen because of its excellent shear strength. It has outstanding resistance to corrosion and generally, used for welding of 5000 series of Aluminium.

3.1.4 ER4047:

It has more silicon than its homologue, ER4043. This allows for more fluidity and less shrinkage in the weld. ER4047 produces bright and almost smut-free welds. This alloy may be used in applications of sustained elevated temperatures.

3.2 COMPOSITION

Chemical composition of various materials used in present research is shown in Table in 3.1:

Table 3.1: Composition of materials used in research

Materials	Si	Fe	Cu	Mn	Mg	Zn	It	Cr	Al
AA6082	0.9	0.1	0.03	0.7	0.9	0.1	0.06	0.20	Remainder
ER4043	4.5-6	0.8	0.30	0.05	0.05	0.10	0.20	0.15	Remainder
ER5356	0.25	0.40	0.10	0.5-1.0	4.7-5.5	0.25	0.05-0.20	0.05-0.20	Remainder
ER4047	13	0.8	0.3	0.15	0.10	0.20	0.05	0.15	Remainder

3.3 APPLICATIONS OF AA6082

AA6082 Aluminium alloy is widely used in applications like high stress applications, Trusses, Bridges, Cranes, Beer barrels and Milk churns etc.

3.4 SAMPLE SIZE AND TYPE OF JOINT

The Aluminium alloy AA6082 of specification of dimension 120mm X 70mm X 3mm was produced by shearing machine. Based on previous literature, Lap joint is not much successful for AA6082 welded joint of less thickness and hence butt joint is selected for proper weldment and higher strength.

3.5 DEVELOPMENT OF GTAW WELDING SYSTEM

In present study tungsten inert gas welding was employed for joining of AA6082 Aluminium alloy due to its simplicity, flexibility in adaption and neatness. This process is also considered unlike GMAW it eliminates the need for mechanical wire feeding, which might pose feed ability concerns. Instead, the welder feeds the filler material into the puddle with his hand. As per the study conducted by researchers it has been concluded that welding of Aluminium alloys depend upon various parameters like welding current, heat input, shielding gas, voltage, filler material and welding speed.

3.5.1 Selection of Process Parameters

Based on the various literature survey, it has been concluded that welding electric current, gas flow rate of argon and filler material are the factors which prominently affect the quality of welded joint, therefore these factors are taken in consideration as a process parameter in present study and decided to perform experiment by employing various combination of these parameters. Taguchi Design of experiments method was used to perform the experiments with different combination of factors and levels.

3.5.2 Design of experiments:

Design of experiments is a statistical tool to build relationships between the process's process variables and the process's output parameters. It's used in both manufacturing and non-manufacturing businesses. It is a widely used instrument in fields such as medicine, engineering, biology, and physics.

Ronald A. Fisher is credited with creating a new way in comparison to the current traditional method by doing agricultural research with the goal of enhancing crop yield in the late 1920s. He then authored a book on DOE in which he explained how the end outcome of an experiment can be determined based on the input components. In a summary, the purpose of design of experiments is to assess a hypothesis' cost effectiveness and process efficiency.

3.5.3 Taguchi orthogonal array design:

Genichi Taguchi, a Japanese engineer, proposed some experimental designs known as "Taguchi designs," which include two-level, three-level, and mixed-level designs. Taguchi orthogonal array (OA) design is a type of factorial design. It is a highly fractional orthogonal design that is based on the matrix proposed by Taguchi which allows to consider multiple factor combinations at different levels.

Available Taguchi Designs (with Number of Factors)

	Single-level designs			
Designs	**2 level**	**3 level**	**4 level**	**5 level**
L4	2-3			
L8	2-7			
L9		2-4		
L12	2-11			
L16	2-15			
L16			2-5	
L25				2-6
L27		2-13		
L32	2-31			

Single-level | Mixed 2-3 level | Mixed 2-4 level | Mixed 2-8 level

Figure 3.1: Available Taguchi Designs for various levels

In general, taguchi design of experiments consists of the following steps as shown in the table below:

Table 3.2: Steps involved in Taguchi design

Steps	Description
Brainstorming	Determine the number of components and levels involved in reaching the process's goal.
Designing experiments	Decide the required orthogonal array and the order of the design runs.
Running experiments	Run experiments in random order as possible.
Analyzing results	Determine the best design and performance under ideal conditions.

Three distinct criteria are accessible to fulfil the specific goal of the study analysis, as shown in the table below:

Table 3.3: Available criteria for Taguchi analysis in Minitab

SIGNAL TO NOISE RATIO	AIM OF THE EXPERIMENT	DATA CHARACTERSTICS	S/N RATIO FORMULAS
Larger the better	Maximize the response	Positive	$\mathbf{S/N = -10 * \log(\Sigma(1/Y^2)/n)}$
Smaller the better	Minimize the response	Non negative with a target value of zero	$\mathbf{S/N = -10 * \log(\Sigma(Y^2)/n))}$
Nominal the best	Target the response as close as possible to standard deviation	Positive, zero or negative	$\mathbf{S/N = -10 * \log(\sigma^2)}$

Where, Y = Responses for the given factor level combination

n = Number of responses in the factor level combination

3.6 EXPERIMENTAL SETUP

Various combinations of process parameters have been employed to conduct the test runs by modifying one of the process parameters and keeping the others unchanged. After exploring appearance of bead and depth of penetration working range of process parameters have been decided. Table 2 shows the operating range of process parameters used in this study. 3 number of Process Parameters were taken for the study and the level of individual parameters is 3. L9 Taguchi Orthogonal array was selected with filler wire ER 4047, ER4043 and ER5356 and experiments were carried out accordingly, hence, total 27 samples (9 samples with each filler wire) were welded by TRITON 220 AC/DC welding machine shown in figure 3.2 by following L9 orthogonal array illustrated in table 3.4.

Figure 3.2: TRITON 220 AC/DC GTAW welding machine

Table 3.4: Operating Range of Process Parameters

Symbols	**Process parameters**	**Unit**	**Lower level**	**Higher-level**
C	Current	Ampere	130	170
FR	Filler rod diameter	Mm	1.6	3.2
G	Gas flow rate	Lt/min	10	14

Table 3.4: L9 Orthogonal Array, Factors=3 and Levels=3

S.no	**C (A)**	**FR (mm)**	**G (Lt/min)**
1	130	1.6	10
2	130	2.4	12
3	130	3.2	14
4	150	1.6	12
5	150	2.4	14
6	150	3.2	10
7	170	1.6	14
8	170	2.4	10
9	170	3.2	12

Before performing welding operation on specimen, AA6082 sheets were cleaned by sand paper to remove the oxide layer. To keep the alignment and spacing, the sheets were kept on a steel backing bar and the ends were clamped. and then welding operation was performed using argon as a shielding gas by following table experimental arrangement presented in table.

Welded sample with filler wire ER4043, ER4047 and ER5356 are shown in below images:

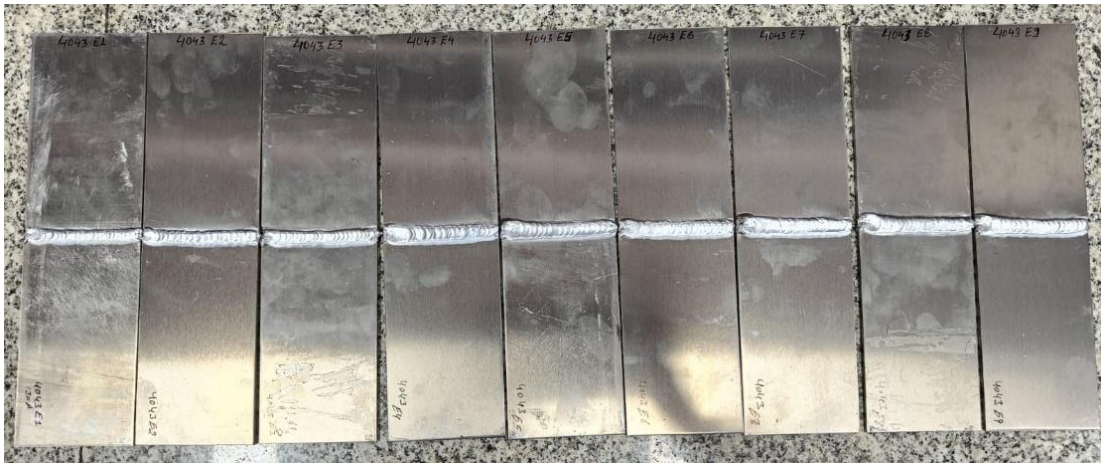

Figure 3.3: Welded specimen using filler ER4043

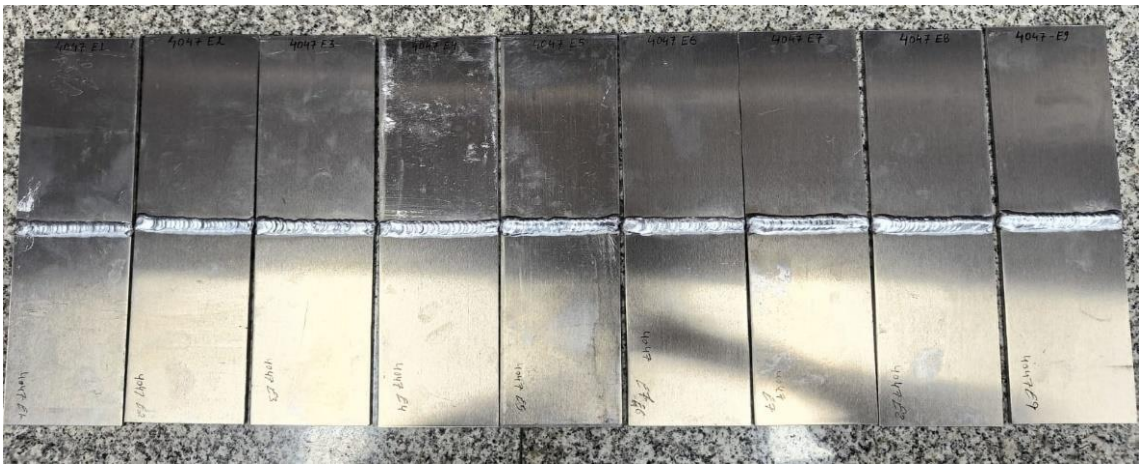

Figure 3.4: Welded specimen using filler ER4047

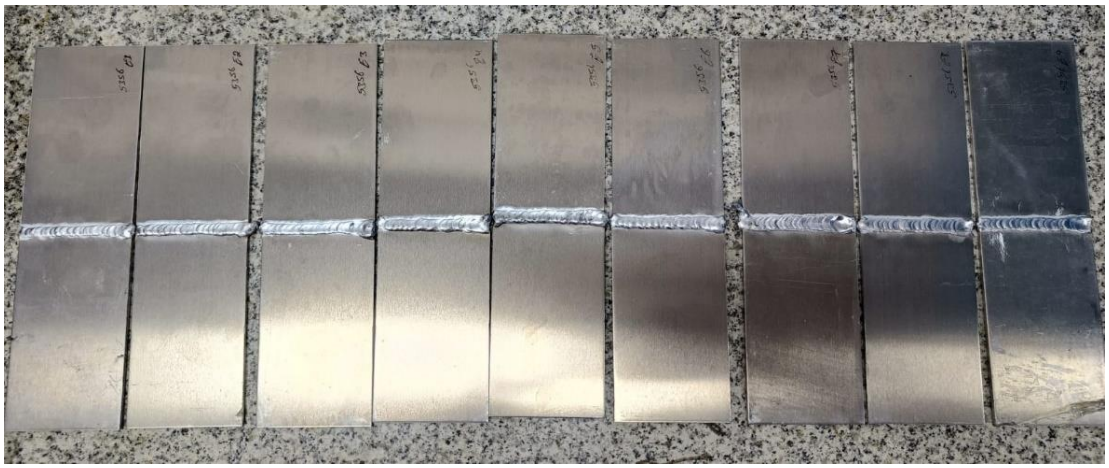

Figure 3.5: Welded specimen using filler ER5356

3.7 CHARECTERIZATION OF WELDED JOINT

3.7.1 TENSILE TEST:

Tensile test of AA6082 welded joint is being done to know about the characteristic of welded specimen under tension load. In tensile test to evaluate the ultimate tensile strength of a material, a sample is routinely tugged to its breaking point. The value of applied force on the specimen and elongation of specimen are calculated throughout the test and presents in terms of stress and strain, values of stress and strain are illustrated on X-Y plot known as stress strain curve.

.

The laser cutting technique, shown in figure 3.6, was employed to form specimens having a weld line in the middle of specimens. ASTM E-8M Standard was followed to design the sample for tensile test. Specimen according to ASTM E8M standard is illustrated in figure 3.7.

Figure 3.6: Laser cutting machine

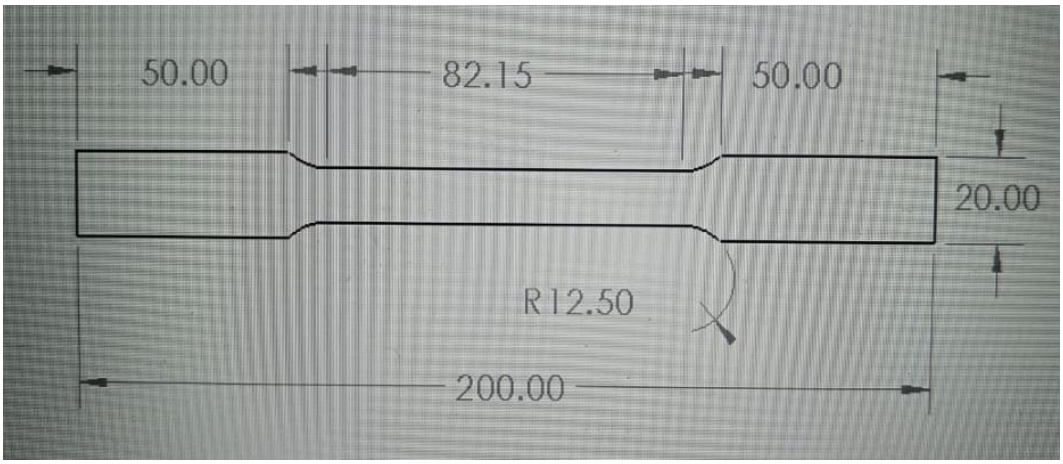

Figure 3.7: Specimen design as per ASTM E8M standard

Specimen with filler wire 4043,4047 and 5356 for tensile test created by laser cutting machine is illustrated in below images:

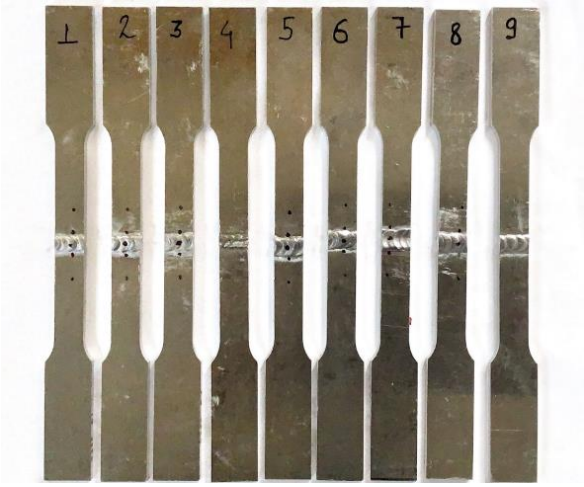

Figure 3.8: tensile test specimen with 4043

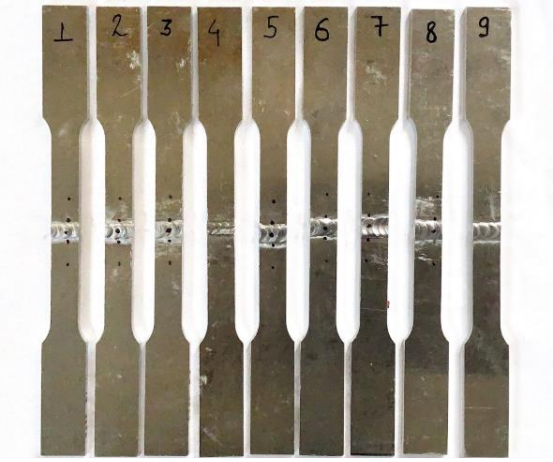

Figure 3.9: tensile test specimen with 4047

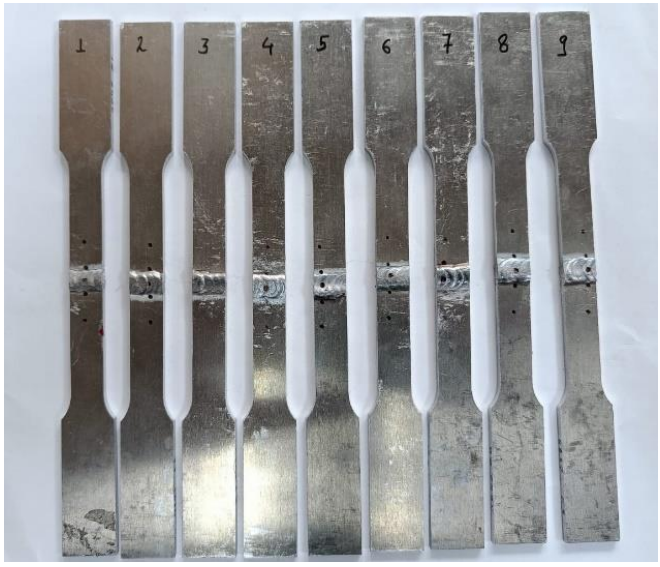

Figure 3.10: tensile test specimen with 5356

Computer-controlled Universal testing machine of 50KN Tones Capacity as manifested in figure 3.11 was used to perform tensile test. Cross speed of 2.54 mm/min was taken for each sample. The tensile test is performed by grasping the end of the specimen in a tensile testing machine and pulling on it until it cracks.

Ultimate tensile strength, off set of yield strength, Stress stain curve, Force extension curve and percentage elongation is also calculated by the machine.

Ultimate tensile strength of welded samples with different filler wires are illustrated in table 3.5.

Figure 3.11: 50KN Capacity UTM

Table 3.5: Quality characteristic data of UTS with each filler wire

S.NO	C (A)	FR (mm)	G (Lt/min)	UTS(MPa) with ER4043	UTS(MPa) With ER4047	UTS(MPa) With ER5356
1	130	1.6	10	69.1	80.1	92.6
2	130	2.4	12	79	71.3	87.3
3	130	3.2	14	67.7	95.6	67.6
4	150	1.6	12	137	155	109
5	150	2.4	14	158	107	121
6	150	3.2	10	142	181	118
7	160	1.6	14	144	157	187
8	160	2.4	10	179	158	110
9	160	3.2	12	129	112	131

3.7.2 RESIDUAL STRESS

Residual stresses are locked in stress present in weld even when there is no external loading. Residual stresses develop in welded material due to differential volumetric change, and differential expansion and contraction. Analysis of residual stress is important in the present study of welding because Fatigue life, Distortion, corrosion resistance, and dimensional stability of welded joints are determined by residual stresses. Generally, both tensile and compressive nature of residual stress exist in welded material. As, per the various researches, tensile residual stress exists at weld bead and heat affected area and compressive residual stress exist at parent metal.

In present study residual stress of optimized sample of each filler is investigated by employing PULSTEC micro-360n X-ray Diffraction machine, which works on the principle of nondestructive X-ray diffraction technique based on cosα method of measuring residual stress .X-ray diffraction technique is used in present study because it makes the measurement process small, simple and easy to access. PULSTEC micro-360n X-ray Diffraction is illustrated in figure 3.11.

Figure 3.11: PULSTEC micro-360n X-ray Diffraction

3.7.2.1 Process of measurement of residual stress-

- A portable X-ray machine (micro-X360) is used to detect residual stress.
- Three markings are made on the surface of the optimized welded sample with each filler wire in order to assess the residual stress as shown in figure 3.12
- First marking is done at parent metal and refer as 1, second marking was done at heat affected area and referred as 2 and third marking was done at weld bead and referred as 3.
- Under the laser, the sample is placed on the V-block.
- The laser is used to focus the collimator on the specimen in order to irradiate the indicated point.
- Diffraction-peak location and stress values are recognized and recorded after a certain amount of time has passed.

Figure 3.12: Marking on welded sample to measure residual stress

3.7.3 OPTICAL MICROSCOPE ANALYSIS

The main objective of optical microscopy is to investigate the microstructure of welded joint and get the idea of change in structure of joint at weld bead, heat affected area and parent metal due to welding.

Microstructure analysis was also employed in present study because it governs strength and service life of welded joint.

Welded specimen with each filler wire having highest tensile strength were selected for the study of microstructure. Hence total 3 samples were selected for this study. Steps involved in preparation of sample for microscopic study are as follows:

- Cutting a piece of 5mm width and 20 mm length from weldment.
- Now create a mold with the use of adhesive and resin to fix the above piece in it.
- Now polish it with different range of emery paper starting from grade 200 to 2600, as shown in figure 3.13
- After getting polished up to grade 2600, wet polishing is performed to get proper surface finish.
- After wet polishing samples are shown in figure 3.14
- Final step in preparation of sample is etching to expose the grains so that it could be easily visible to microscope. Etching is performed with Keller's reagent with an idle time of 15 to 20 seconds
- OLYMPUS LG-PS2 as shown in figure 3.15 optical microscope was used to analyze the microstructure.

Figure 3.13: Polishing of sample by emery paper

Figure 3.14: Samples after wet polishing

Figure 3.15: OLYMPUS PS2 Optical microscope

3.7.4 MICROHARDNESS ANALYSIS

Micro-indentation hardness testing (also known as micro hardness testing) is a technique for determining a material's hardness on a small scale. At loads ranging from a few grams to one kilogramme, a precision diamond indenter is impressed into the material. A hardness value is

calculated using the microscopically recorded impression length and the test load. The obtained hardness values are good indications of a material's characteristics and predicted service life.

Weld specimens having highest tensile strength with each filler wire are selected for hardness testing, hence total 3 samples are selected for hardness test.

Vickers hardness testing DRAMIN-40 STRUERS is employed to perform hardness Test. Vickers hardness testing machine has a Vickers indenter shown in figure 3.16 which is pressed into the material's surface with specific force, diagonals of pyramid shape indentation are measured with the help of microscope to evaluate the hardness value of specimen.

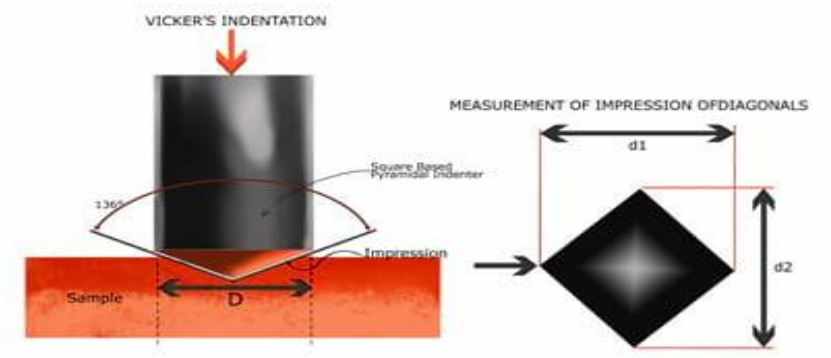

Figure 3.16: Pyramid shape indenter of Vickers hardness testing machine

Vickers hardness test was performed at a load of 500 gram and dwell time for indentation is kept 10 second. Hardness values taken from the center of Weld pool to base metal news are plotted on the graph of hardness versus distance from the center. Vickers hardness testing machine DRAMIN-40 STRUERS is illustrated in figure 3.17

Figure 3.17: DRAMIN-40 STRUERS hardness testing machine

CHAPTER 4

RESULT AND DISCUSSION

Aluminium AA6082 alloy has been joined with the help of ER4043, ER4047 and ER5356 at different set of parameters. The main focus is to find out the most optimum levels of process parameter with each filler fire, using Taguchi method and ANOVA analysis. To further study the quality of welded joints different test has been performed on the optimized specimens of each filler wire.

4.1 OPTIMIZATION USING TAGUCHI TECHNIQUE:

Design and analysis of experiments to perform Taguchi technique, ANOVA has been done by using Minitab software. The logical interface of Minitab makes it easy to use and its features make it easy to get desired results.

Taguchi technique is an experimental procedure to reduce the attempts of tests in comparison to long-established techniques. It comes up with an anticipated model to find the most appropriate process parameters.

The Present research focus on getting the maximum ultimate tensile strength of the TIG-welded joint of AA 6082 alloy.

Taguchi L9 Orthogonal array is employed to perform the experiments in present study. A separate L9 orthogonal array has been created for welding samples with each filler wire with 3 factors (welding current, Filler rod diameter, gas flow rate) and 3 levels of each factor. Ultimate tensile strength of each welded joint is taken as response variable. Present research uses a larger is better S/N ratio characteristic of the Taguchi method. Rank of each parameter influencing the ultimate tensile strength is also determined by Taguchi technique.

Table 4.1: L9 Orthogonal array, UTS of weld specimen with each filler wire as response variable

S.NO	C (A)	FR (mm)	G (Lt/min)	UTS(MPa) with ER4043	UTS(MPa) With ER4047	UTS(MPa) With ER5356
1	130	1.6	10	69.1	80.1	92.6
2	130	2.4	12	79	71.3	87.3
3	130	3.2	14	67.7	95.6	67.6
4	150	1.6	12	137	155	109
5	150	2.4	14	158	107	121
6	150	3.2	10	142	181	118
7	160	1.6	14	144	157	110
8	160	2.4	10	179	158	187
9	160	3.2	12	129	112	131

4.1.1 Analysis of variance-

The motive of using the analysis of variance (ANOVA) test in our research is to find the effect of individual parameter on the response variable i.e. ultimate tensile strength. The ANOVA also tells which process parameter is most statistically significant. ANOVA table results for UTS of the welded joint of AA6082 alloy with each filler material.

ANOVA table has been created for weld specimens with each filler wire.

4.1.1.1 Optimization of weld specimen with ER4043 filler wire:

As per the taguchi optimization of welded samples with ER4043 filler wire, the best level of process parameters with the largest S/N ratio, which indicate the maximum tensile strength, is found at welding current at level 3 (170A), filler road diameter at level 2 (2.4mm) and gas flow rate at level 1(10 Lt/min).

The plot of the S/N ratio against the design factors is shown in figure 4.1 and response for the S/N ratio is shown in Table 4.2.

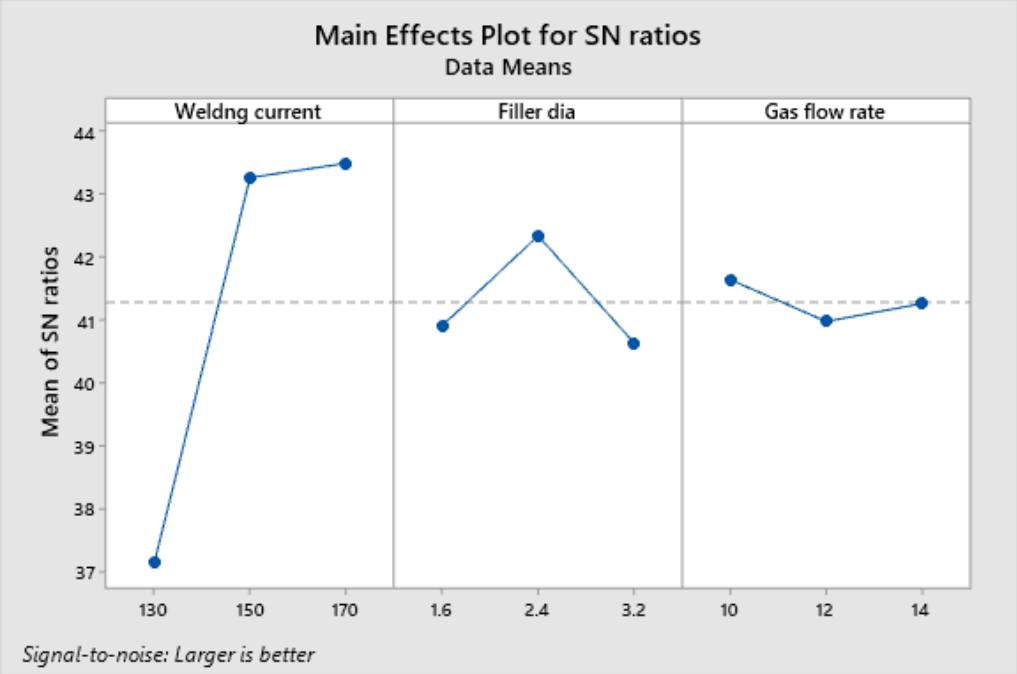

Figure 4.1: Main effects plot between S/N ratio and current, filler diameter, gas flow rate of weld specimen with 4043

Table 4.2: Response for the signal to noise ratio (Larger is better) with 4043

Level	Welding current	Filler diameter	Gas flow rate
1	37.12	40.90	41.63
2	43.25	42.33	40.97
3	43.48	40.62	41.25
Delta	6.36	1.70	0.66
Rank	1	2	3

- **Analysis of variance for weld specimen with ER4043 filler material.**

Table 4.3: ANOVA table for UTS with filler 4043

Source	DF	Seq SS	Adj SS	Adj MS	F-Value	P-Value
Welding current	2	11660.5	11660.5	5830.27	88.14	0.011
Filler rod diameter	2	1160.9	1160.9	580.45	8.78	0.102
Gas flow rate	2	340.0	340.0	170.01	2.57	0.280
Error	2	132.3	132.3	66.15		
Total	8	13293.8				

Table 4.4: Model summary for UTS with filler 4043

S	R-sq	R-sq(adj)	PRESS	R-sq(pred)	BIC
8.13313	99.00%	96.02%	2678.98	79.85%	67.31

In ANOVA, a Comparison of the value of each factor is used to find the significance of the control factors. When the F ratio has a greater value as welding current in the present research, then the response variable can be significantly affected by a change in that particular welding process parameter. P-value for an F test is a statistical measurement that authenticates a hypothesis against observed results. P-value computes the probability of getting the observed results, taking null hypothesis is true, for the model to be the significant value of P should be as small as possible.

As per table, which indicates that the value of P foe welding electric current is less than 0.05 (0.011) that means welding electric current is the factor which individually most important factor for the welding process of AA6082 alloy with ER4043.

Table. model summary indicates R-sq is a validation criterion, which means that in this example, the model accounts for 78.37% of the variance in the predictor, or strength

4.1.1.2 Optimization of weld specimen with ER4047 filler wire:

As per the taguchi optimization of welded samples with ER4047 filler wire, the best level of process parameters with the largest S/N ratio, which indicate the maximum tensile strength, is found at welding current at level 2 (150A), filler road diameter at level 3 (3.2mm) and gas flow rate at level 1(10 Lt/min).

The plot of the S/N ratio against the design factors is shown in figure 4.2 and response for the S/N ratio is shown in Table 4.5.

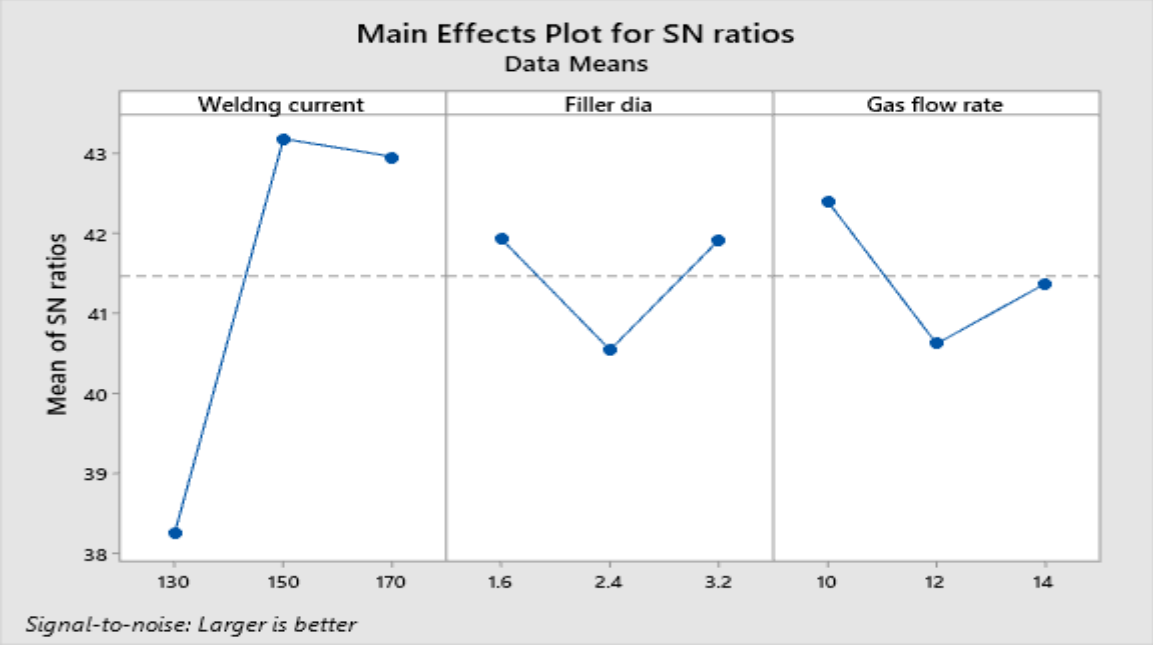

Figure 4.2: Main effects plot between S/N ratio and current, filler diameter, gas flow rate of weld sample with 4047

Table 4.5: Response for the signal to noise ratio (Larger is better) with 4047

Level	Welding current	Filler diameter	Gas flow rate
1	38.25	41.93	42.40
2	43.18	40.54	40.62
3	42.96	41.92	41.37
Delta	4.93	1.39	1.78
Rank	1	3	2

- **Analysis of variance for weld specimen with ER4047 filler material.**

Table 4.6: ANOVA Table for UTS with 4047

Source	DF	Seq SS	Adj SS	Adj MS	F-Value	P-Value
Welding current	2	7896.9	7896.9	7896.9	2.94	0.0253
Filler rod diameter	2	651.2	651.2	651.2	0.24	0.805
Gas flow rate	2	1169.2	1169.2	1169.2	0.44	0.696
Error	2	2681.6	2681.6	2681.6		
Total	8	12398.9		12398.9		

Table 4.7: Model summary for UTS with 4047

S	R-sq	R-sq(adj)	PRESS	R-sq(pred)	BIC
36.6172	78.37%	13.49%	54303.3	0.00%	94.39

Table illustrated ANOVA table for welded specimen with ER4047 which indicates the value of P is less than 0.05 (0.0253) for welding electric current process parameter therefore, response variable can be significantly affected by a change in electric current welding process parameter.

Table. model summary indicates R-sq is a validation criterion, which means that in this example, the model accounts for 78.37% of the variance in the predictor, or strength.

4.1.1.3 Optimization of weld specimen with ER5356 filler wire:

As per the taguchi optimization of welded samples with ER5356 filler wire, the best level of process parameters with the largest S/N ratio, which indicate the maximum tensile strength, is found at welding current at level 3 (170A), filler road diameter at level 2 (2.4mm) and gas flow rate at level 1(10 Lt/min).

The plot of the S/N ratio against the design factors is shown in figure 4.3 and response for the S/N ratio is shown in Table 4.8.

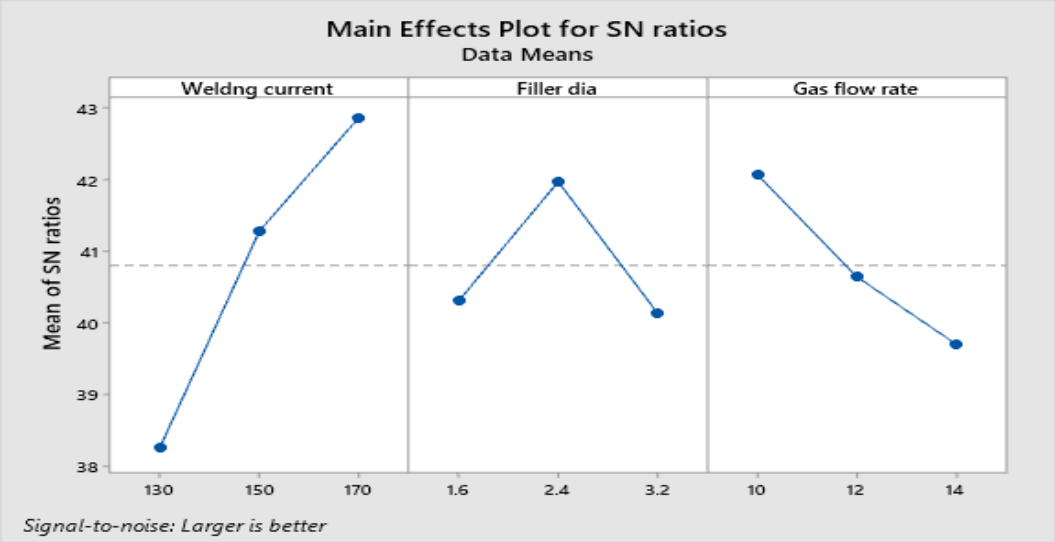

Figure 4.3: Main effects plot between S/N ratio and current, filler diameter, gas flow rate of weld sample with 5356

Table 4.8: Response for the signal to noise ratio (Larger is better) with 5356

Level	Welding current	Filler diameter	Gas flow rate
1	38.25	40.30	42.07
2	41.28	41.97	40.64
3	42.87	40.13	39.69
Delta	4.62	1.84	2.37
Rank	1	3	2

- **Analysis of variance for weld specimen with ER5356 filler material.**

Table 4.9: ANOVA table for UTS with 5356

Source	DF	Adj SS	Adj SS	Adj MS	F-Value	P-Value
Welding current	2	5453.4	5453.4	2726.7	13.82	0.067
Filler rod diameter	2	1469.4	1469.4	734.7	3.72	0.212
Gas flow rate	2	1729.6	1729.6	864.8	4.38	0.186
Error	2	394.7	394.7	197.4		
Total	8	9047.1				

Table 4.10: Model summary for UTS with 5356

S	R-sq	R-sq(adj)	PRESS	R-sq(pred)	BIC
14.0483	95.64%	82.55%	7992.86	11.65%	77.15

Table illustrated ANOVA table for welded specimen with ER4047 which indicates the value of P is less than 0.05 (0.067) for welding electric current process parameter therefore, response variable can be significantly affected by a change in electric current welding process parameter.so, welding electric current is the most important process parameter which affects the strength of TIG welded specimen of AA6082 alloy with ER5356.

Table. model summary indicates R-sq is a validation criterion, which means that in this example, the model accounts for 95.64% of the variance in the predictor, or strength.

From the experimental investigation and use of Taguchi technique, ANOVA method it has been concluded that welding electric current is the most prominent process parameter for the maximum tensile strength og GTAW welded joint of AA6082 alloy with each filler wire . Optimum level of process parameters for maximum tensile strength of TIG welded AA6082 welded specimen is illustrated below:

FOR ER4043-C(170A), FR(2.4mm), GF (10lt/min) and UTS- 179MPa

FOR ER4047- C(170A), FR(3.2mm), GF (10lt/min) and UTS-181MPa

FOR ER5356-C(170A), FR(2.4mm), GF (10lt/min) and UTS-187 MPa

4.2 TENSILE TEST ANALYSIS-

Tensile testing is performed to check the strength of welded joint. All 27 samples (9 samples with each filler wire) has undergone tensile test. As, discussed earlier sample for tensile test is designed asper ASTM E8M standard.

Analysis of tensile test of welded specimen with each filler wire is discussed below:

4.2.1 Tensile test analysis of welded specimen with filler ER4043:

All the 9 welded samples of filler wire ER4043 have undergone tensile test. Out of 9 welded samples some of the samples failed from the welded zone, some from the heat affected zone and some from base metal.

Maximum tensile strength comes out to be 179MPa (will refer it as E8), when AA6082 alloy is welded with filler wire ER4043.The level of process parameter at maximum tensile strength is current at 170 ampere, diameter of filler rod is 2.4mm and flow rate of argon gas is 10 Lt/min.

Above values of process parameters suggested that on increasing the welding current there is significant improvement in penetration of liquid metal into the roots of specimens which results in higher strength of joint.

Optimum level of gas flow rate is recommended to prevent the heat losses and oxidation but higher level of argon gas flow rate is not suggested because it would cause cooling and turbulence in the weld pool.

Figure 4.4: fractured welded samples of ER4043

E8 welded sample of filler wire ER4043 fractured from the base metal which means integrity of welding is satisfactory that is why out of all 9 samples of ER4043 E8 sample is having maximum strength, fractured E8 sample is shown in figure 4.5. Stress strain graph diagram of welded sample of filler ER4043, having highest tensile strength (i.e. 179MPa) is shown in figure 4.6 and has been discussed in detail.

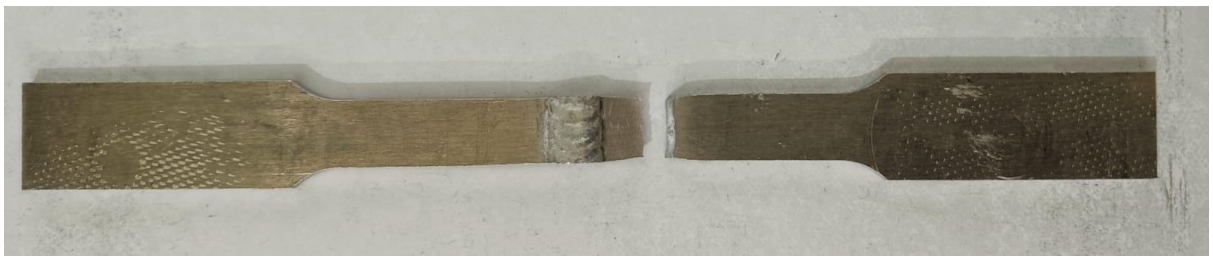

Figure 4.5: Fractured weld specimen E8 of ER4043

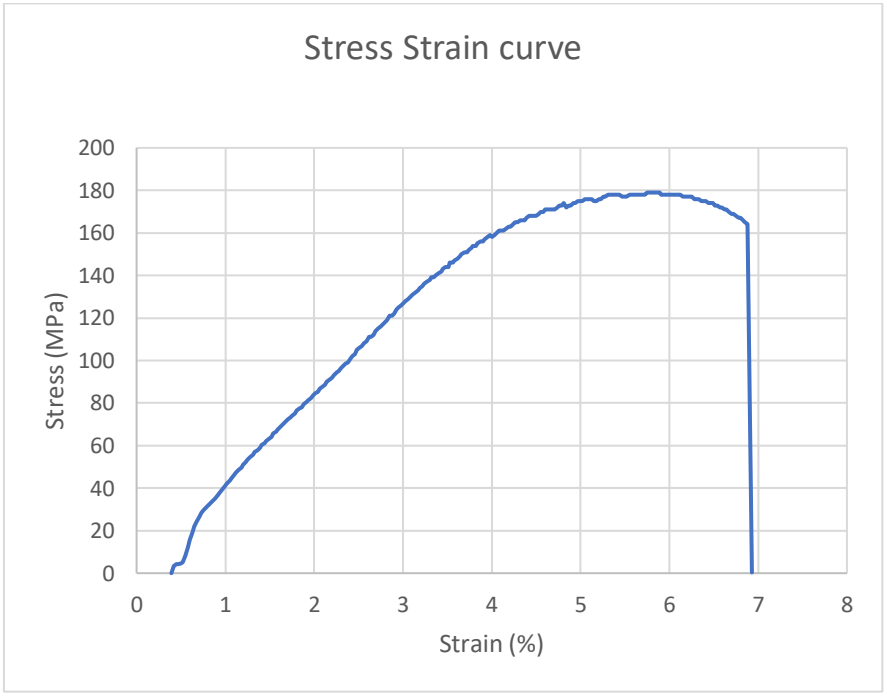

Figure 4.6: Stress Strain curve of E8 welded sample of ER4043

Above Stress strain graph of E8 sample of filler wire ER4043 illustrate that Ultimate tensile strength comes out to be 179MPa.Initially gauge length of specimen was 82.15mm and failure occurs at 87. 5mm.Hence Elongation percentage comes out to be 6.88 %.

4.2.2 Tensile test analysis of welded specimen with filler ER4047:

All the 9 welded samples of filler wire ER4047 have undergone tensile test. Out of 9 welded samples some of the samples failed from the welded zone, some from the heat affected zone and some from base metal.

Maximum tensile strength comes out to be 181MPa (will refer this sample as E6), when AA6082 alloy is welded with filler wire ER4043.The level of process parameter at maximum

tensile strength is current at 150 ampere, diameter of filler rod is 3.2mm and flow rate of argon gas is 10 Lt/min.

Above values of process parameters suggested that on increasing the welding current there is significant improvement in penetration of liquid metal into the roots of specimens which results in higher strength of joint.

Optimum level of gas flow rate is recommended to prevent the heat losses and oxidation but higher level of argon gas flow rate is not suggested because it would cause cooling and turbulence in the weld pool.

Figure 4.7: fractured welded samples of ER4047

E6 welded sample of filler wire ER4047 fractured from the base metal which means integrity of welding is satisfactory that is why out of all 9 samples of ER4047, E6 sample is having maximum strength, fractured E6 sample is shown in figure 4.8.

Stress strain diagram of welded sample of filler ER4043, having highest tensile strength (i.e. 181MPa) is shown in figure 4.9 and the graph has been discussed in detail.

Figure 4.8: Fractured weld specimen E6 of ER4047

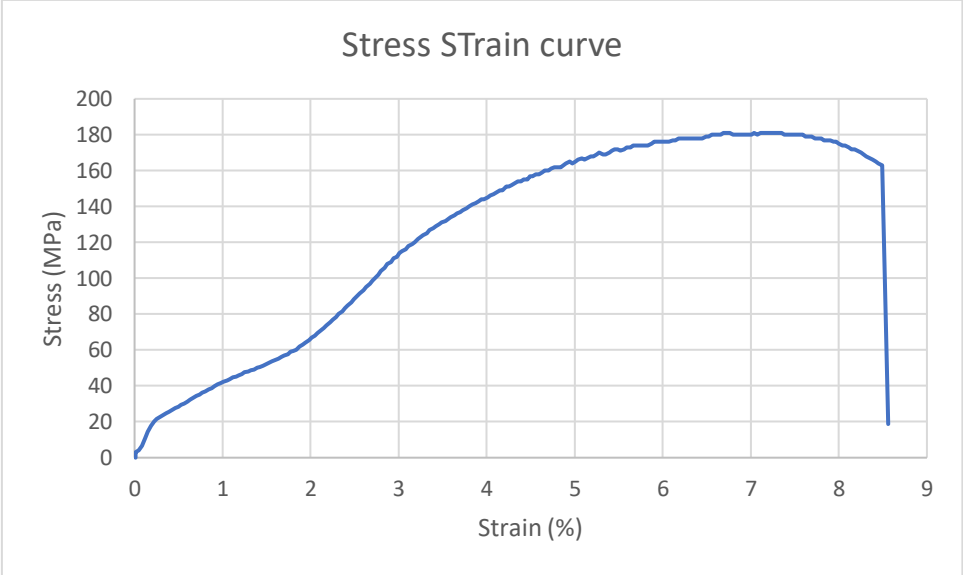

Figure 4.9: Stress Strain curve of E6 welded sample of ER4047

Above Stress strain graph of E6 sample of filler wire ER4047 illustrate that Ultimate tensile strength comes out to be 181MPa.Initially gauge length of specimen was 82.15mm and failure occurs at 89.2mm.Hence Elongation percentage comes out to be 8.49 %.

4.2.3 Tensile test analysis of welded specimen with filler ER5356:

All the 9 welded samples of filler wire ER5356 have undergone tensile test. Out of 9 welded samples some of the samples failed from the welded zone, some from the heat affected zone and some from base metal.

Maximum tensile strength comes out to be 187MPa (will refer this sample as E8), when AA6082 alloy is welded with filler wire ER5356.The level of process parameter at maximum tensile strength is current at 170 ampere, diameter of filler rod is 2.4mm and flow rate of argon gas is 10 Lt/min.

Tensile test results of AA6082 welded specimen with filler ER5356 reveals that on increasing the welding current there is significant improvement in penetration of liquid metal into the roots of specimens which results in higher strength of joint.

Optimum level of gas flow rate is recommended to prevent the heat losses and oxidation but higher level of argon gas flow rate is not suggested because it would cause cooling and turbulence in the weld pool.

Image of all the 9 samples weld by Gas tungsten arc welding with filler wire ER5356 is illustrated in figure 4.10

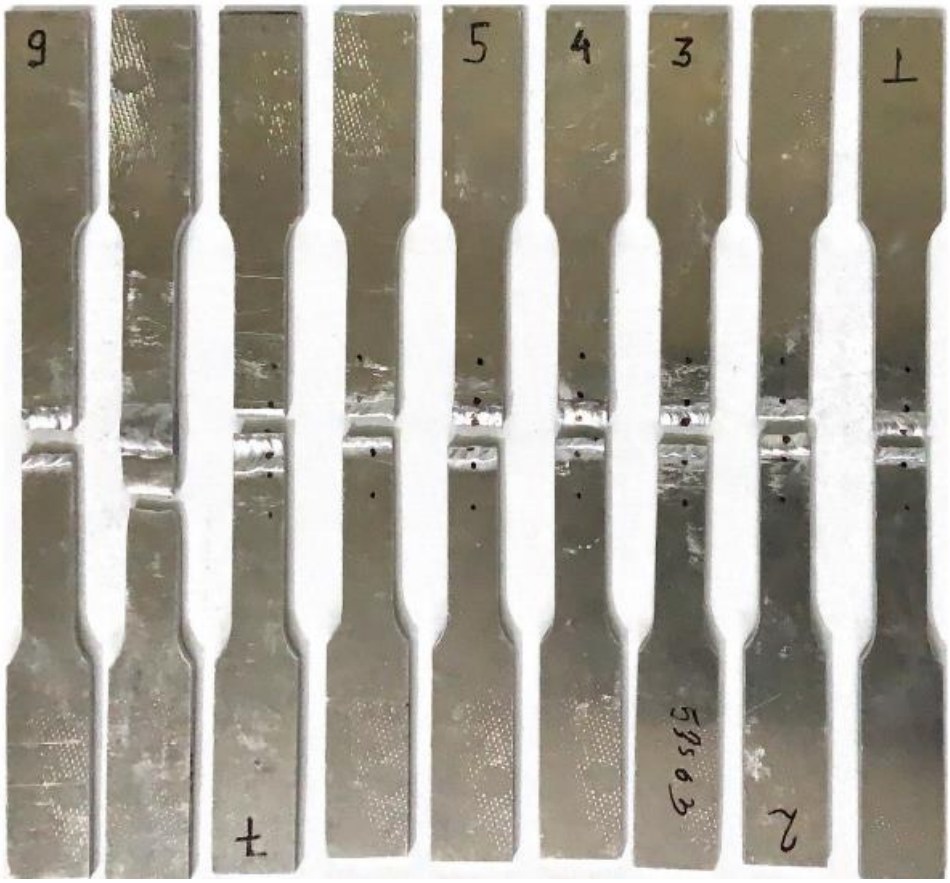

Figure 4.10: fractured welded samples of ER5356

E8 welded sample of filler wire ER5356 fractured from the base metal which means integrity of welding is satisfactory that is why out of all 9 samples of ER5356, E8 sample is having maximum strength, fractured E8 sample is shown in figure 4.11

Stress strain diagram of welded sample of filler ER5356, having highest tensile strength (i.e. 187MPa) is shown in figure 4.12 and the graph has been discussed in detail

Figure 4.11: Fractured weld specimen E8 of ER5356

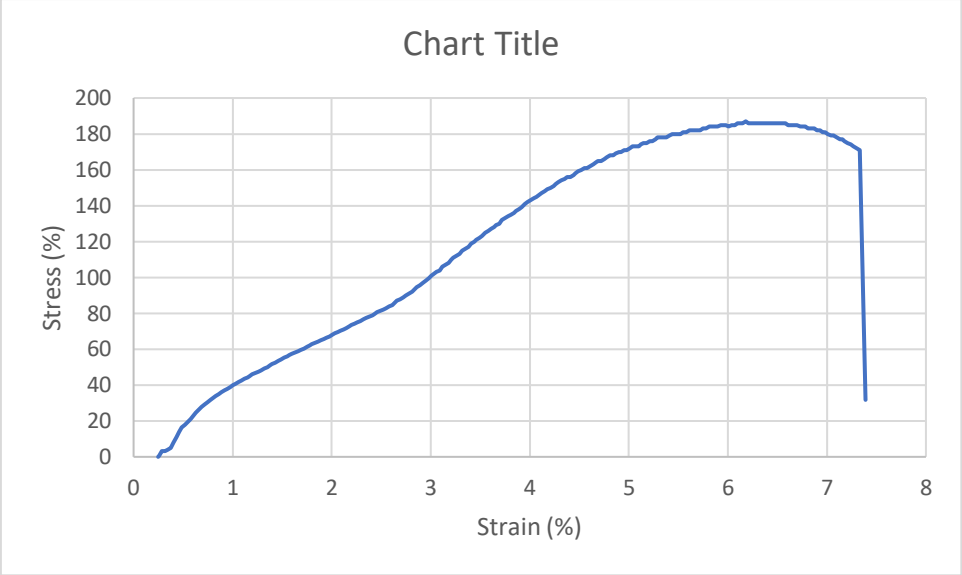

Figure 4.12: Stress Strain curve of E8 welded sample of ER5356

Above Stress strain graph of E8 sample of filler wire ER5356 illustrate that Ultimate tensile strength comes out to be 187MPa.Initially gauge length of specimen was 82.15mm and failure occurs at 88mm.Hence Elongation percentage comes out to be 7.33 %.

After performing tensile test of each weld specimen with Filler wires 4043,4047 and 5356, Maximum tensile strength of GTAW welded AA6082 Aluminium alloy comes out to be 187MPa when welded by ER5356 filler wire.

4.3 RESIDUAL STRESS ANALYSIS:

As discussed earlier residual stresses are locked in stress when there is no loading. They occur frequently during the welding process; generally tensile stress exists at the weld bead and compressive stress exist at base metal [8]. Tensile residual stress is detrimental to the component [9], but compressive stress can be beneficial in many situations.

Residual stress has both pros and cons on welding parts, with compressive residual stress typically showing a better or helpful effect. Scientists discovered that residue can minimize fatigue crack formation and propagation, as well as improve corrosion rate. prolong the life of weld joints and avoid stress corrosion cracking problem

In present research for each filler wire residual stress of optimized process parameters welded Specimen has been calculated. Therefore, Total 3 samples are selected for measuring residual stress and for comparison.

At 3 points residual stress has been measured and these points are base metal (refer as point 1), heat affected zone (refer as point 2) and weld bead (refer as point 3).

Residual stress measurement of welded specimen with each filler wire is discussed below:

4.3.1 Residual stress analysis of welded joint with 4043:

At Point 1:

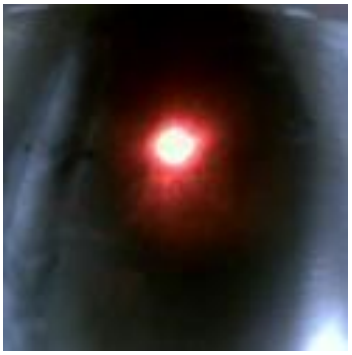

Figure 4.13: Camera image of point 1 of 4043 sample

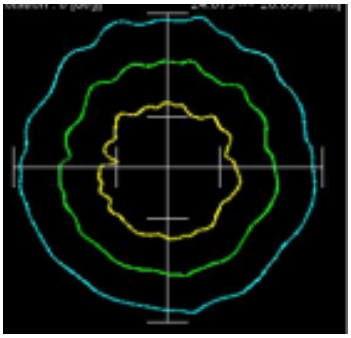

Figure 4.14: Distortion graph of point 1 of 4043 sample

Residual stress

Normal stress= -26MPa

Shear stress= 15MPa

At Point 2:

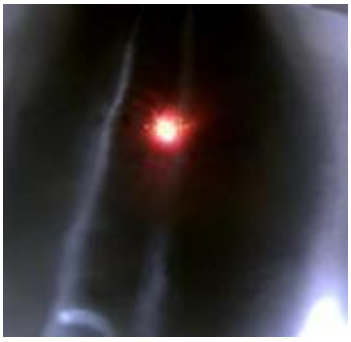

Figure 4.15: Camera image of point 2 of 4043 sample

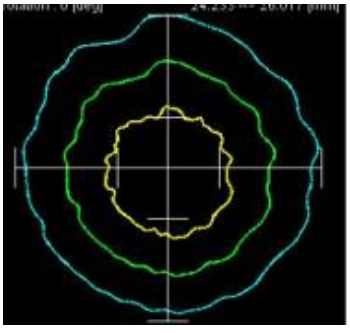

Figure 4.1: Distortion graph of point 2 of 4043 sample

Residual stress

Normal stress= +22MPa

Shear stress= 15MPa

At point 3

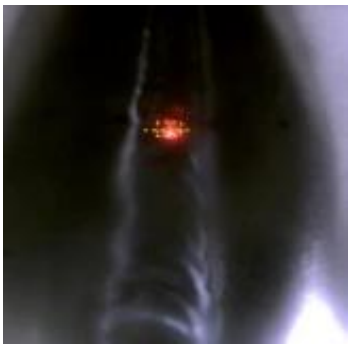

Figure 4.17: Camera image of point 1 of 4043 sample

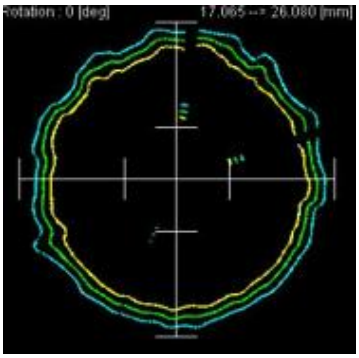

Figure 4.18: Distortion graph of point 3 of 4043 sample

Normal stress= +80MPa

Shear stress= -59MPa

4.3.2 Residual stress analysis of welded joint with 4047

At Point 1:

Figure 4.19: Camera image of point 1 of 4047

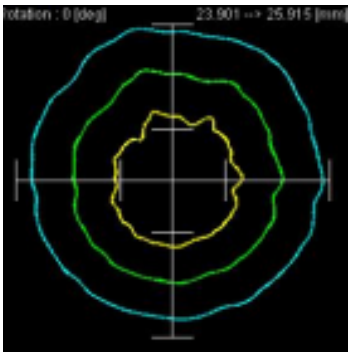

Figure 4.20: Distortion graph of point 1 of 4047

Residual stress

Normal stress= -39MPa

Shear stress= 25MPa

At Point 2:

Figure 4.21: Camera image of point 2 of 4047

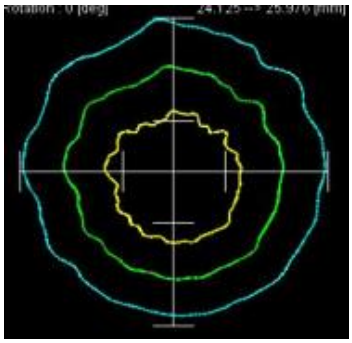

Figure 4.22: Distortion graph of point 2 of 4047

Residual stress

Normal stress= +31 MPa

Shear stress= 08 MPa

At Point 3:

Figure 4.23: Camera image of point 3 of 4047

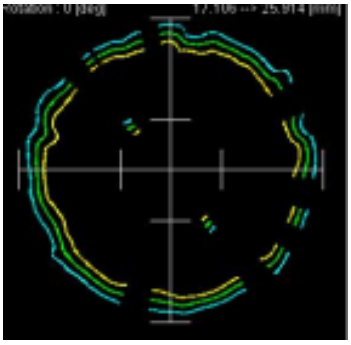

Figure 4.24: Distortion graph of point 3 0f 4047

Residual stress

Normal stress= +190 MPa

Shear stress= -52 MPa

4.3.3 Residual stress analysis of welded joint with 5356:

At Point 1:

Figure 4.25: Camera image of point 1 of 5356

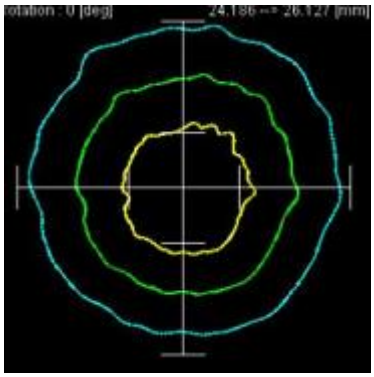

Figure 4.26: Distortion graph of point 1 of 5356

Residual stress

Normal stress= -35 MPa

Shear stress= 17 MPa

At Point 2:

Figure 4.27: Camera image of point 2 of 5356

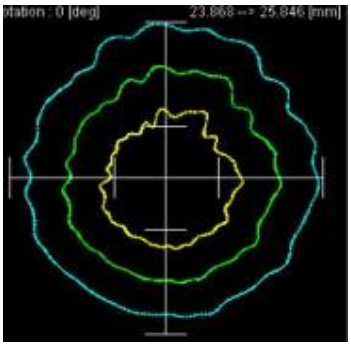

Figure 4.28: Distortion graph of point 2 of 5356

Residual stress

Normal stress= +5 MPa

Shear stress= 34 MPa

At Point 3:

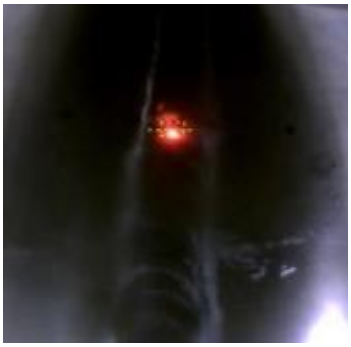

Figure 4.29: Camera image of point 3 of 5356

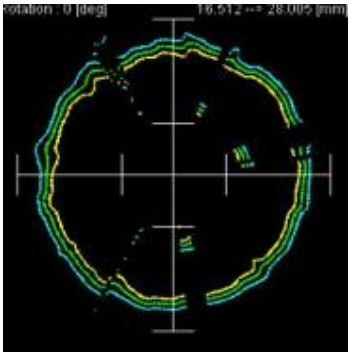

Figure 4.30: Distortion graph of point 3 of 5356

Residual stress

Normal stress= +36 MPa

Shear stress= 6 MPa

From the above investigation and analysis of residual stresses of optimized parameter of each filler wire it has been concluded that compressive nature of residual stress exists at base metal and tensile nature of residual stress exist at weld bead and heat affected area.

The value of tensile residual stress at weld bead is more than the value of residual stress at heat affected area.

The value of residual stress at weld bead of welded specimen with 5356 filler wire has lesser value than the welded specimens with 4043 and 4047. This is also one of the reasons that welded specimen with 5356 filler wire has highest tensile strength.

Above analysis of residual stress revealed that for minimum residual stress in welded joint of AA6082 aluminium alloy welding has to be done with ER5356 filler wire

4.4 MICROHARDNESS TEST

Microhardness analysis is performed on optimized welded specimens of each filler materials i.e. one welded sample of each filler wire. Hardness value is taken from centre of weld bead to the base metal. Three points are selected for testing at each region as shown in figure 4.31

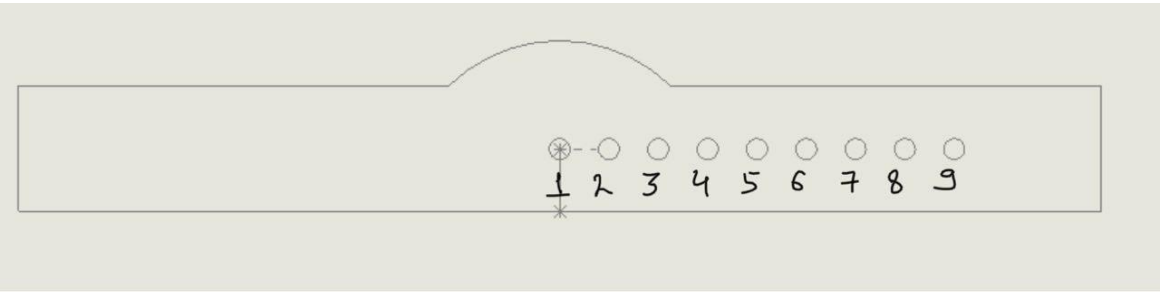

Figure 4.31: Hardness testing points from weld bed to base metal

Hardness analysis of weld specimen of each filler wire is discussed below:

4.4.1 Microhardness analysis of optimized weld specimen of ER4043 filler material.

Optimized process parameter of AA6082 welded specimen is at C(170A), FR(2.4mm), GF (10Lt/min). Here we are referring this sample as E8.

Vickers hardness testing with load of 500gm is employed for testing with indentation time of 10s.Three indentation has been made at each zone. Hence, total 9 indentation has been made on one specimen. Value of hardness are plotted on a graph of hardness vs distance from centre as shown in figure 4.32

Table 4.11 indicates the hardness value of optimized specimen of AA6082 alloy with 4043 at distance from centre. Indentation marks of indentation on metal with their dimension is also illustrated in figure 4.33

Table 4.11: Hardness value of optimized weld specimen with ER4043

S.no.	Distance from centre(mm)	Hardness value HV0.5
1	0	79.06
2	2	77.36
3	4	79.1
4	6	62.96
5	8	68.25
6	10	73.46
7	12	106.63
8	14	108.41
9	16	105.4

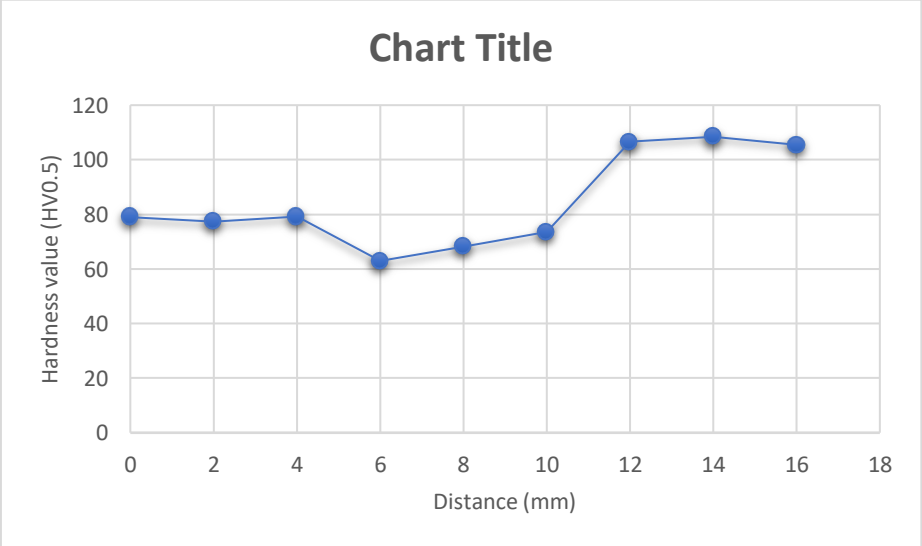

Figure 4.32: hardness vs distance graph of E8 sample of 4043

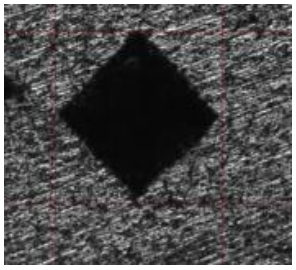

D1 0.1099 mm, D2 0.1133 mm

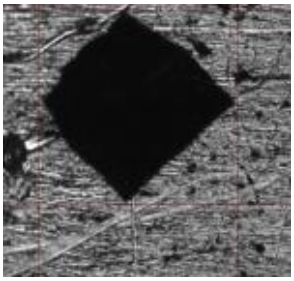

D1 0.1114 mm, D2 0.1076 mm

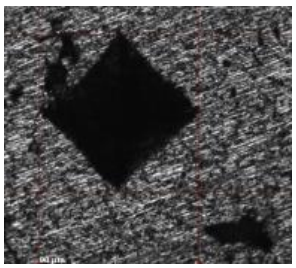

D1 0.1156 mm, D2 0.1133 mm

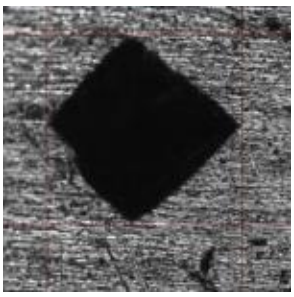

D1 0.1094 mm, D2 0.1072 mm

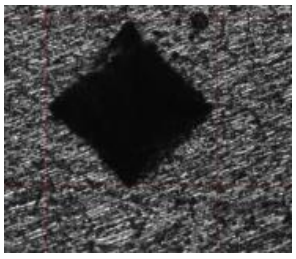

D1 0.1164 mm, D2 0.1133 mm

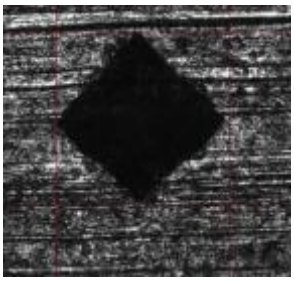

D1 0.0926 mm, D2 0.0939 mm

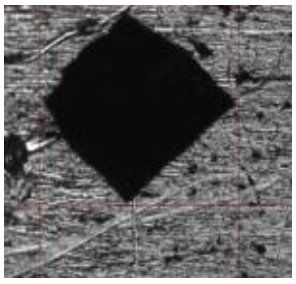

D1 0.1103 mm, D2 0.1063 mm

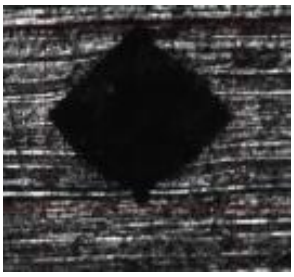

D1 0.0945 mm, D2 0.0904 mm

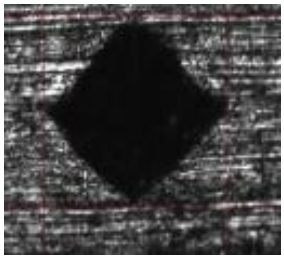

D1 0.0922, D2 0.0954

Figure 4.33: Images and dimension of diamond shape indentation from weld bead to base metal of filler 4043

The maximum value of hardness of aa6082 welded joint with 4043 filler wire comes out to be 108.41HV at base metal. Figure graph between hardness and distance from centre shows that value of hardness decreases from welded zone to heat affected zone and then increases sharply from heat affected zone to base metal.

4.1.2 Microhardness analysis of optimized weld specimen of ER4047 filler material

Optimized process parameter of AA6082 welded specimen is at C(150A), FR(3.2mm), GF (10Lt/min). Here we are referring this sample as E6.

Vickers hardness testing with load of 500gm is employed for testing with indentation time of 10s.Three indentation has been made at each zone. Hence, total 9 indentation has been made on one specimen. Value of hardness are plotted on a graph of hardness vs distance from centre as illustrated in figure 4.34

Table 4.12 indicates the hardness value of optimized specimen of AA6082 alloy with 4047 at distance from centre. Indentation marks of diamond indenter on metal with their dimension is also illustrated in figure 4.35.

Table 4.12: Hardness value of optimized weld specimen with ER4047

S.no.	Distance from centre(mm)	Hardness value HV0.5
1	0	83.33
2	2	81.75
3	4	81.44
4	6	78.49
5	8	69.62
6	10	66.22
7	12	109.33
8	14	107.13
9	16	104.58

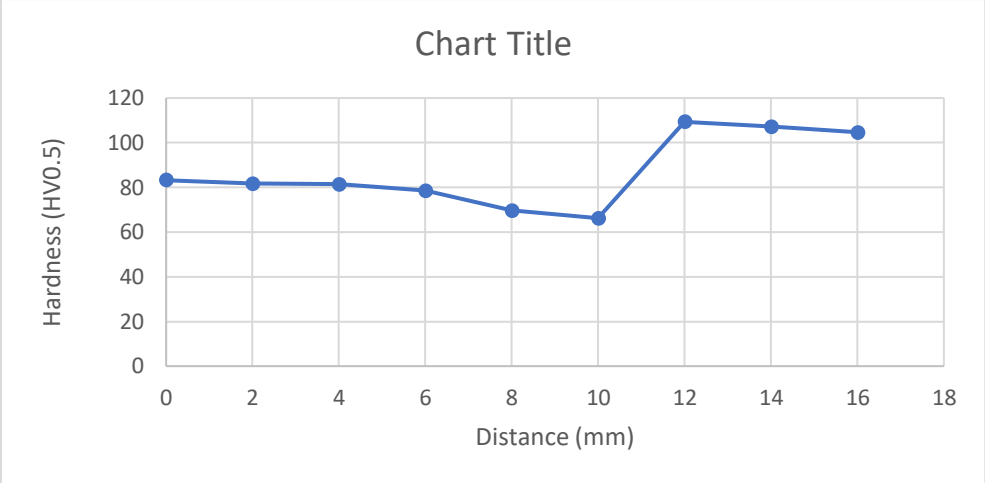

Figure 4.34: hardness vs distance graph of E6 sample of 4047

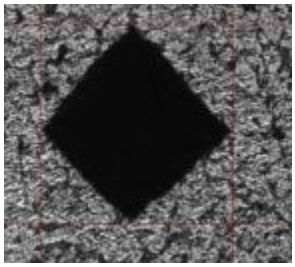

D1 0.1038mm, D2 0.1071mm

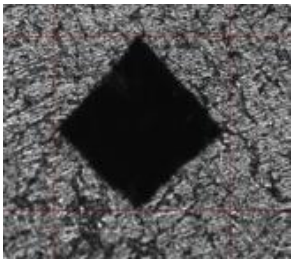

D1 0.1072mm, D2 0.1058mm

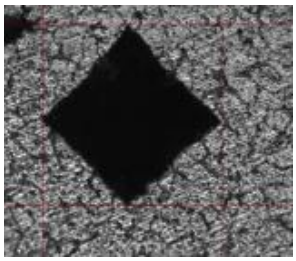

D1 0.1063mm, D2 0.1058mm

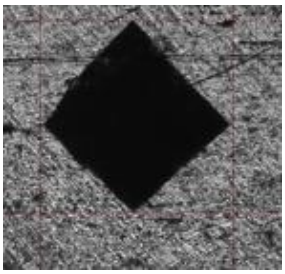

D1 0.1085mm, D2 0.1089mm

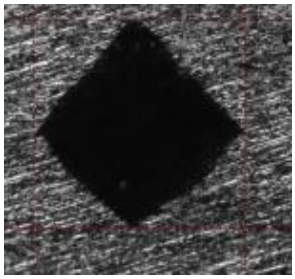

D1 0.1141mm, D2 0.1167mm

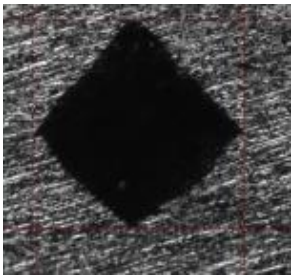

D1 0.1191mm, D2 0.1175mm

D1 0.1094 mm, D2 0.1093 mm

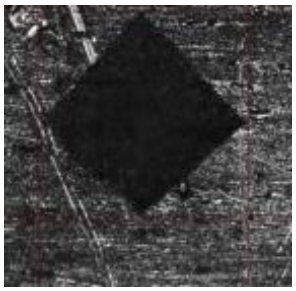

D1 0.1120 mm, D2 0.1111 mm

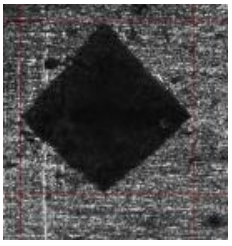

D1 0.1120 mm, D2 0.1100 mm

Figure 4.35: Images and dimension of diamond shape indentation from weld bead to base metal of filler 4047

The maximum value of hardness of AA6082 welded joint with 4047 filler wire comes out to be 107.13HV at base metal. Figure graph between hardness and distance from centre shows that value of hardness decreases from welded zone to heat affected zone and then increases sharply from heat affected zone to base metal.

4.1.3 Microhardness analysis of optimized weld specimen of ER5356 filler material.

Optimized process parameter of AA6082 welded specimen is at C(170A), FR(2.4mm), GF (10Lt/min). Here we are referring this sample as E8.

Vickers hardness testing with load of 500gm is employed for testing with indentation time of 10s.Three indentation has been made at each zone. Hence, total 9 indentation has been made on one specimen. Value of hardness are plotted on a graph of hardness vs distance from centre as illustrated in figure 4.36

Table 4.13 indicates the hardness value of optimized specimen of AA6082 alloy with 5356 at distance from centre. Indentation marks of diamond indenter on metal with their dimension is also illustrated in figure 4.37

Table 4.13: Hardness value of optimized weld specimen with ER5356

S. No.	Distance from centre(mm)	Hardness value HV0.5
1	0	83.27
2	2	84.23
3	4	82.28
4	6	63.81
5	8	63.69
6	10	68.64
7	12	104.48
8	14	107.87
9	16	109.03

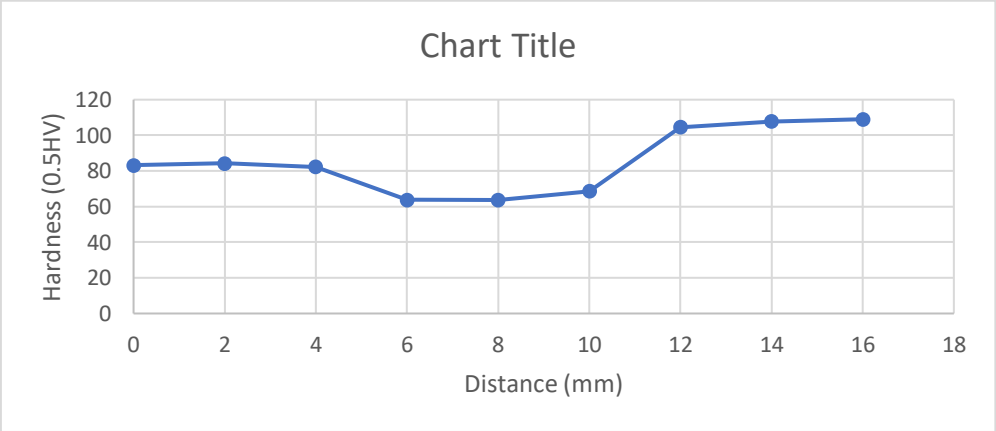

Figure 4.36: Hardness vs distance graph of E8 sample of 5356

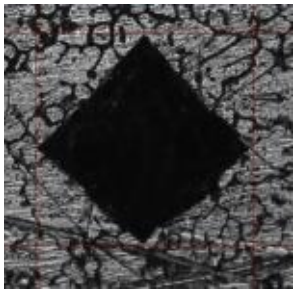

D1 0.1171mm, D2 0.1186mm

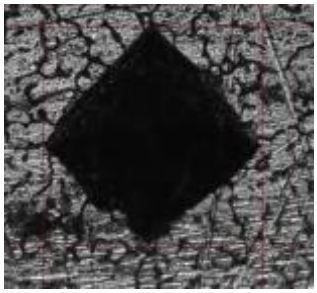

D1 0.1224mm, D2 0.1186mm

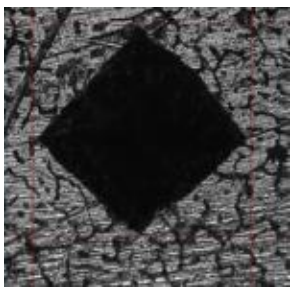

D1 0.1224mm, D2 0.1189mm

D1 0.1094mm, D2 0.1093mm

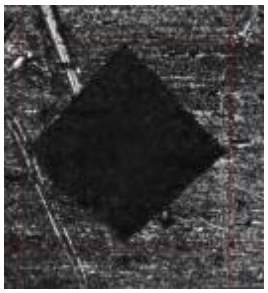

D1 0.1120mm, D2 0.1111mm

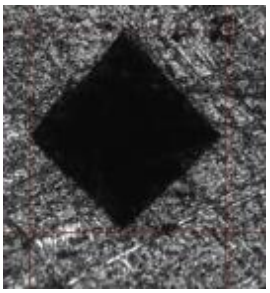

D1 0.1120mm, D2 0.1100mm

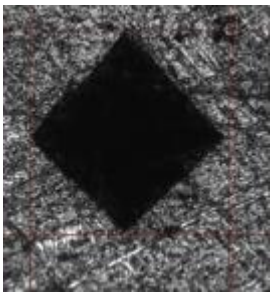

D1 0.1089mm, D2 0.1086mm

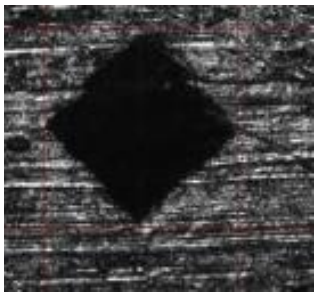

D1 0.1094mm, D2 0.1093mm

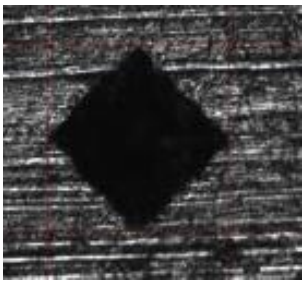

D1 1099mm, D2 1098mm

Figure 4.37: Images and dimension of diamond shape indentation from weld bead to base metal of filler 5356

The maximum value of hardness of AA6082 welded joint with 5356 filler wire comes out to be 109.33HV at base metal. Figure graph between hardness and distance from centre shows that value of hardness decreases from welded zone to heat affected zone and then increases sharply from heat affected zone to base metal

From the above analysis of hardness of AA6082 welded sample with each filler wire it has been revealed that maximum hardness has been found in weld joint with filler wire 4043 followed by weld joint with filler 5356 and minimum hardness found in weld specimen with filler 4047.

4.5 MICROSTRUCTURE ANALYSIS

Microstructure analysis of specimens welded at optimized parameter with each filler wire material has been carried out. Three regions are considered for the study, these regions are base metal, heat affected area and weld bead.

Microstructure study has been done on X100, X200, X500 scale with the help of Olympus microscope

Microscopic images of optimized welded specimens are shown and discussed below

4.5.1 Microstructure images of optimized weld specimen with filler wire 4043

Optimized weld specimen with filler wire 4043 is having process parameter C(170A), FR(2.4mm), GF (10Lt/min). This can be referring as E8, microscopic images of E8 welded specimen at various level of zoon are shown below:

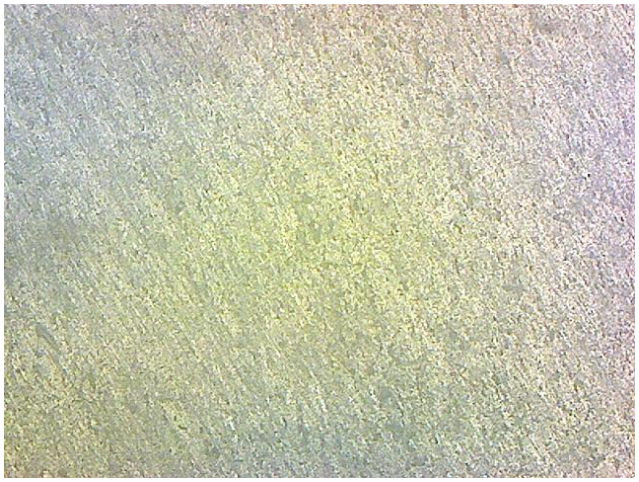

Base metal

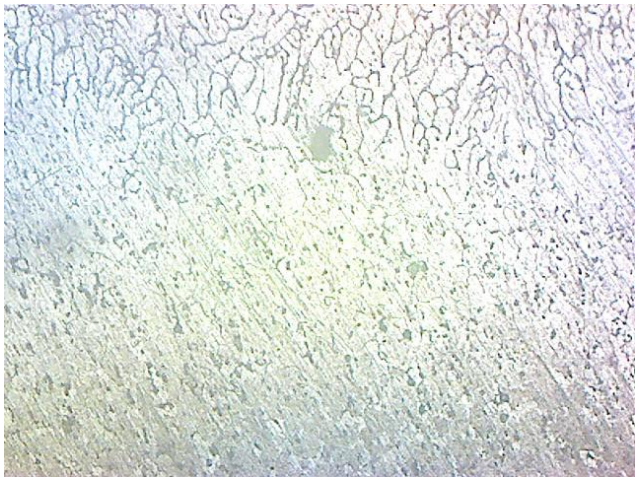

Heat affected area

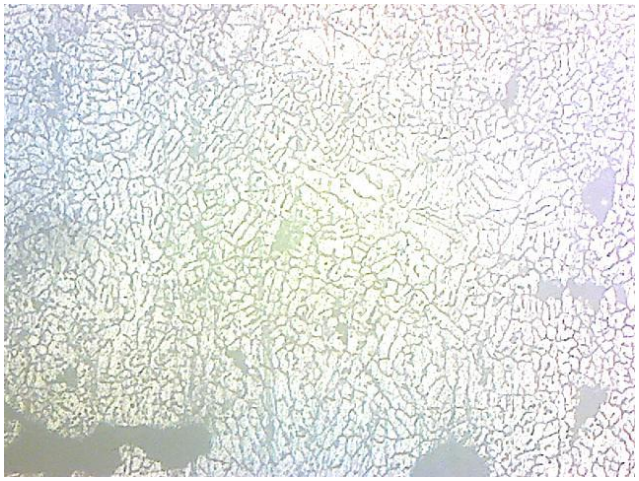

Weld bead

Figure 4.38: Microscopic images of optimized weld sample with ER4043 at X100

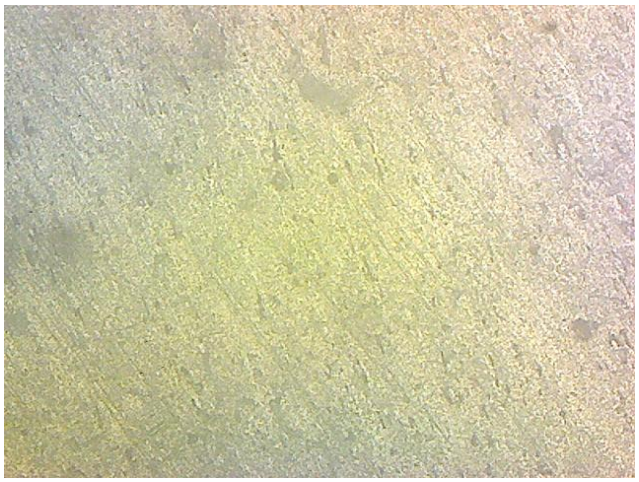

Base metal

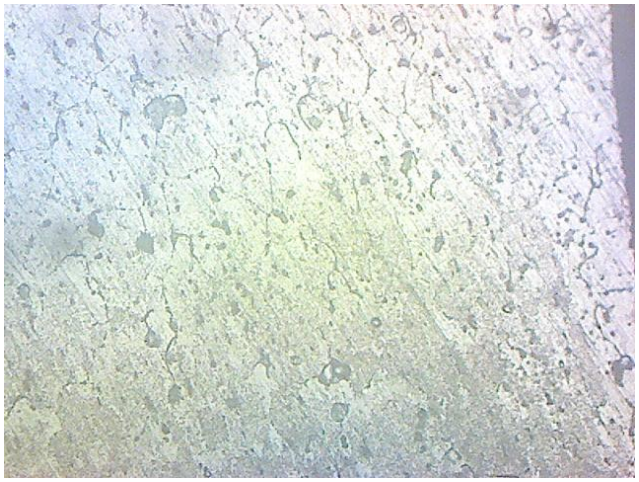

Heat affected area

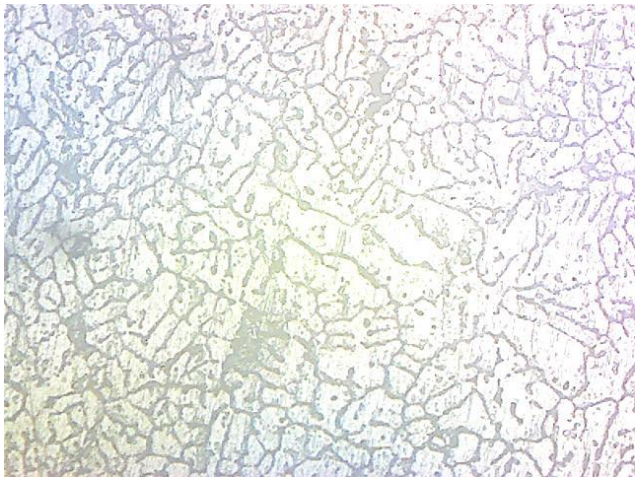

Weld bead

Figure 4.39: Microscopic images of optimized weld sample with ER4043 at X200

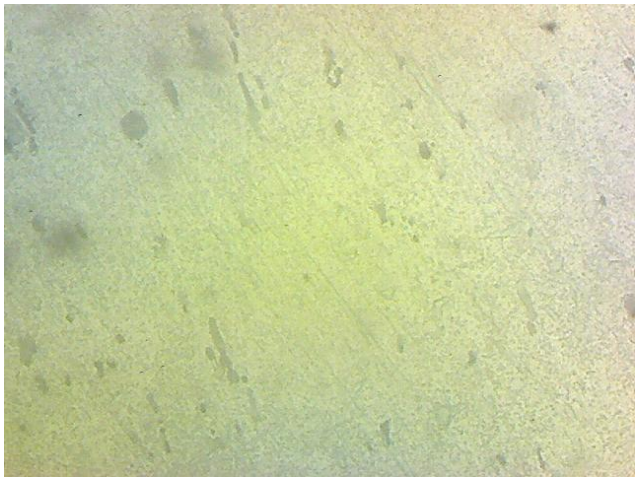

Base metal

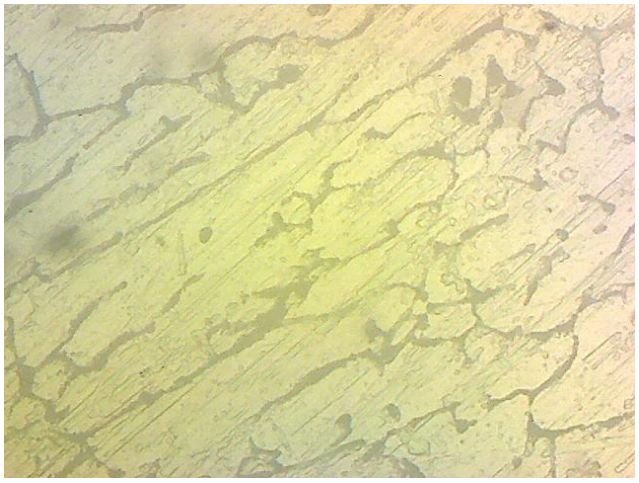

Heat affected area

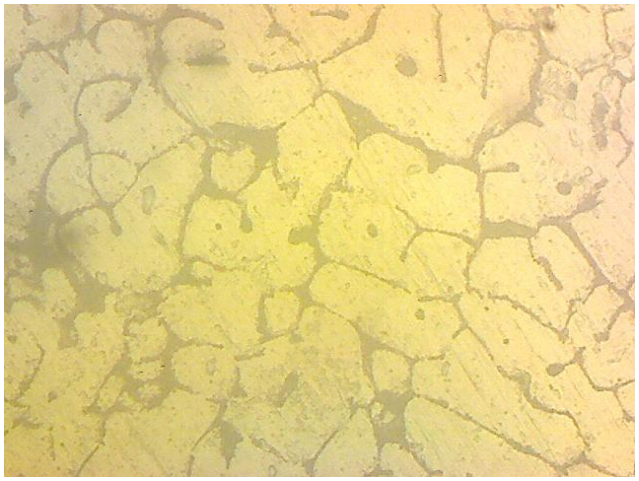

Weld bead

Figure 4.40: Microscopic images of optimized weld sample with ER4043 at X500

4.5.2 Microstructure images of optimized weld specimen with filler wire 4047

Optimized weld specimen with filler wire 4047 is having process parameter C(150A), FR(3.2mm), GF (10Lt/min). This can be referring as E6, microscopic images of E6 welded specimen at various level of zoom are shown below:

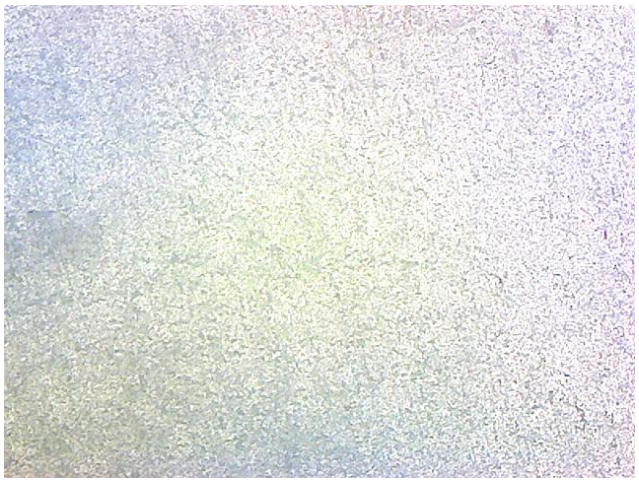

Base metal

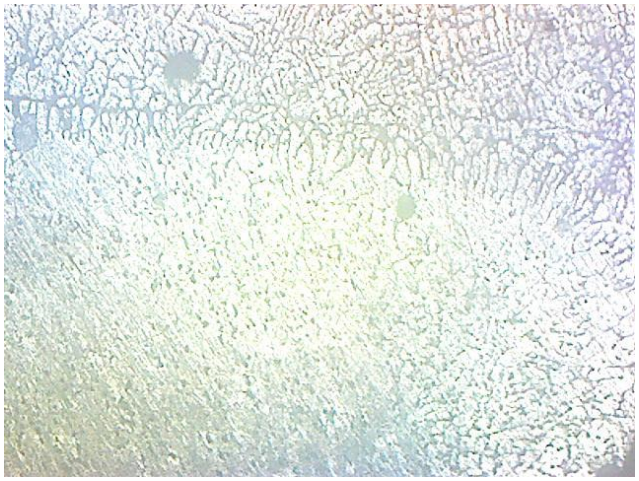

Heat affected area

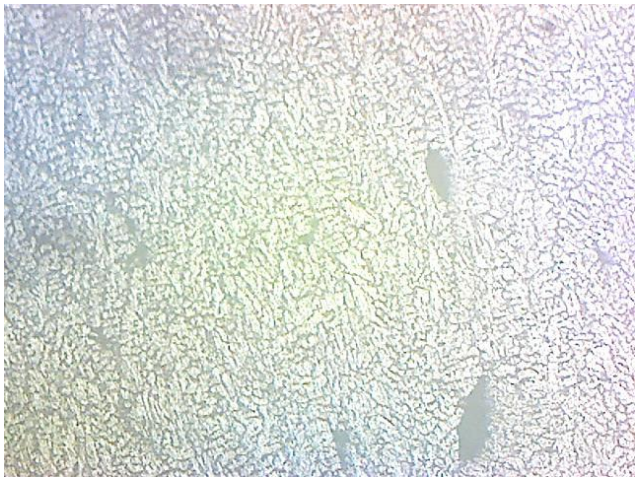

Weld bead

Figure 4.41: Microscopic images of optimized weld sample with ER4047 at X100

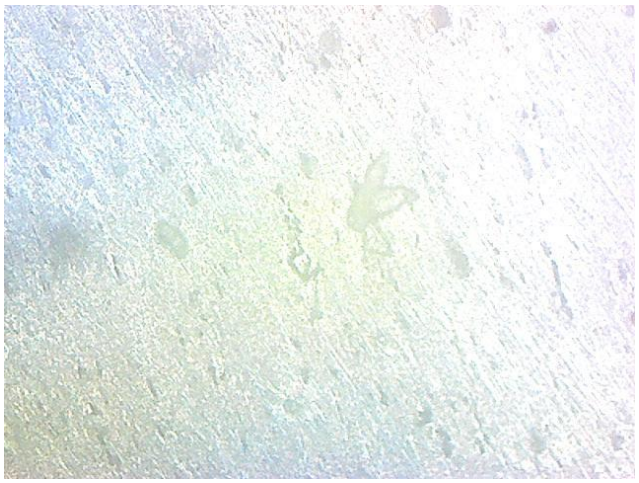

Base metal

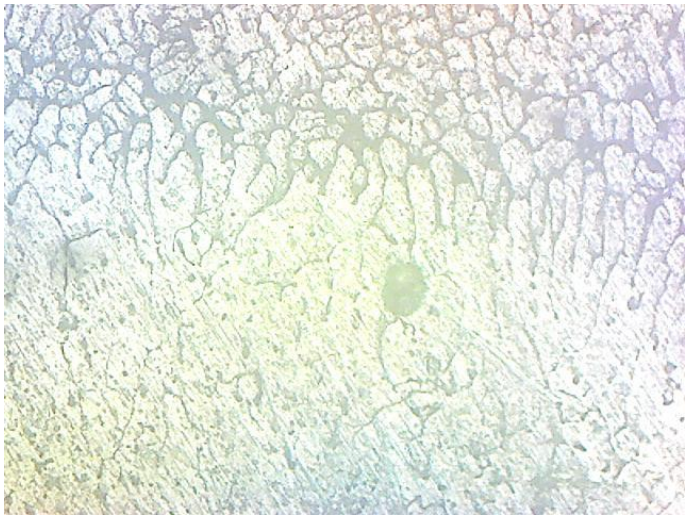

Heat affected area

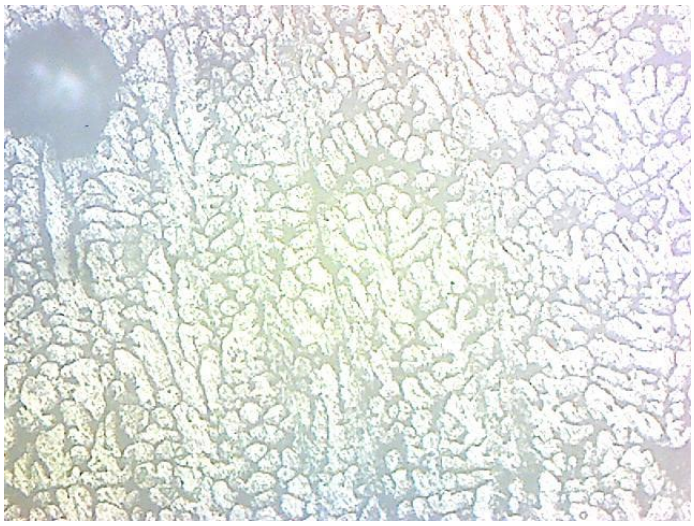

Weld bead

Figure 4.42: Microscopic images of optimized weld sample with ER4047 at X200

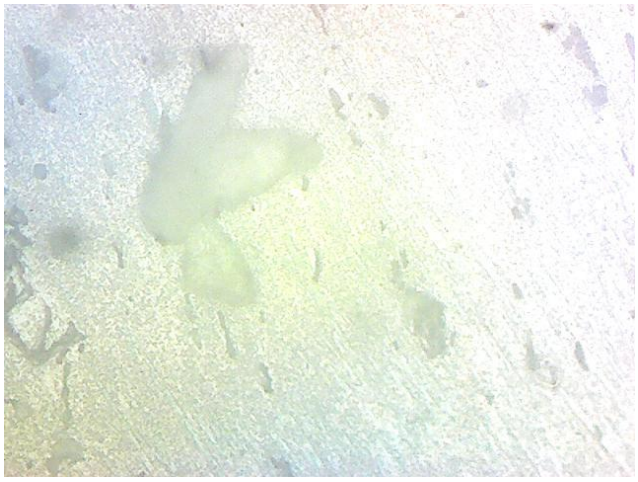

Base metal

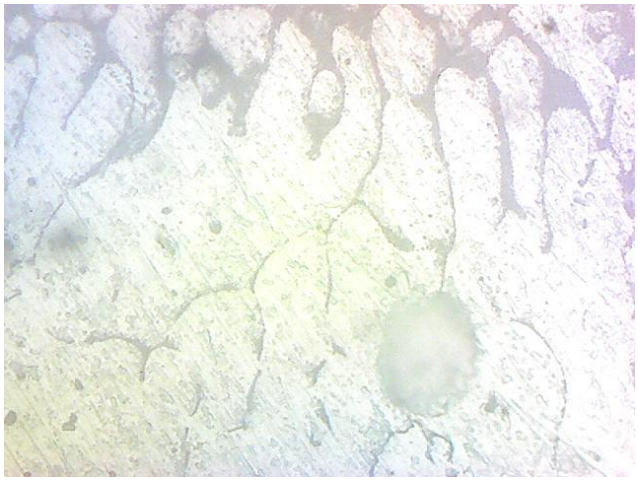

Heat affected area

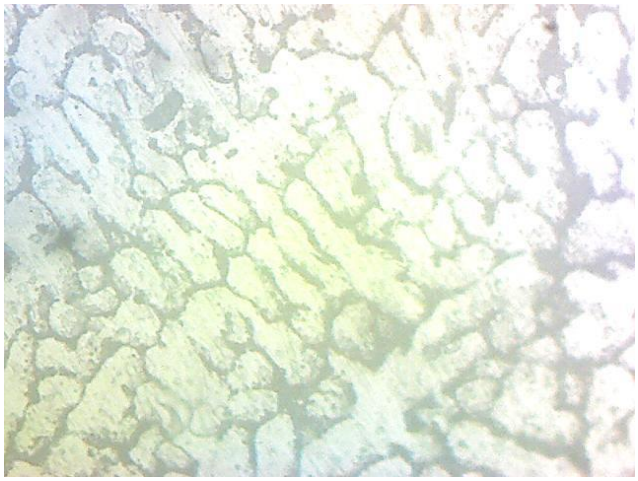

Weld bead

Figure 4.43: Microscopic images of optimized weld sample with ER4047 at X500

4.5.3 Microstructure images of optimized weld specimen with filler wire 5356

Optimized weld specimen with filler wire 5356 is having process parameter C(170A), FR(2.4mm), GF (10Lt/min). This can be referring as E8, microscopic images of E8 welded specimen at various level of zoom are shown below:

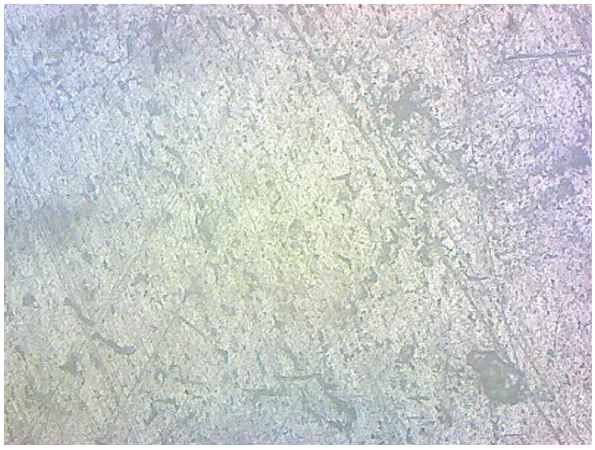

Base metal

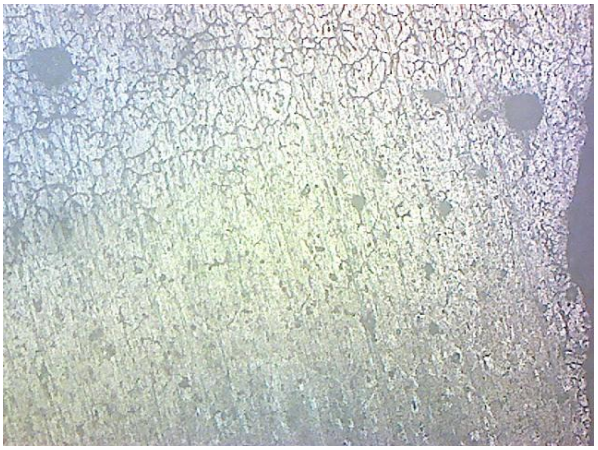

Heat affected area

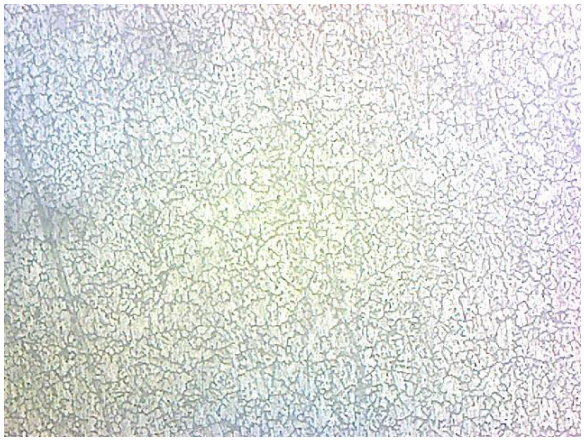

Weld bead

Figure 4.44: Microscopic images of optimized weld sample with ER5356 at X100

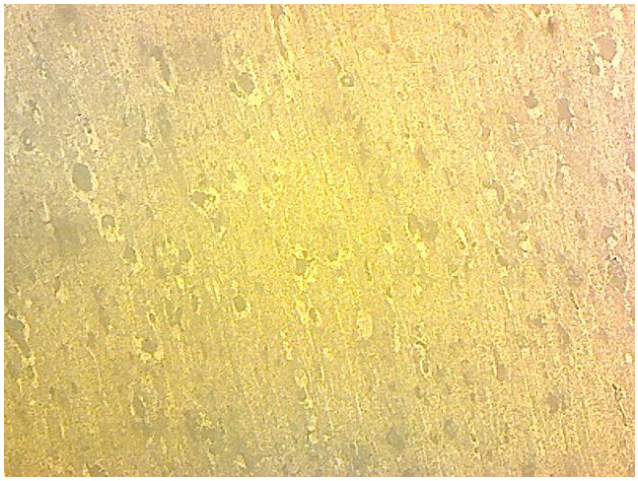

Base metal

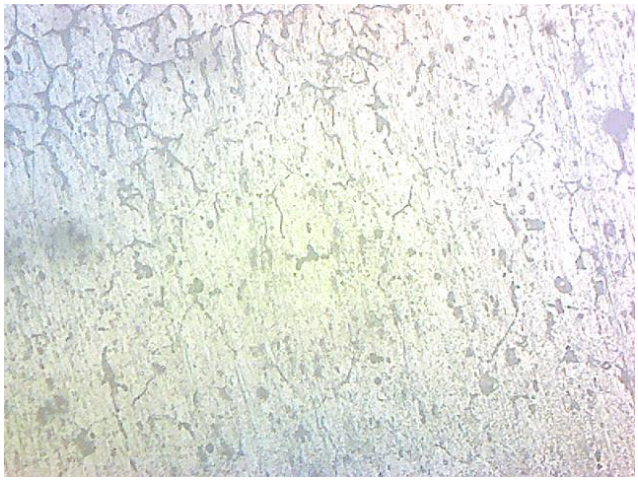

Heat affected area

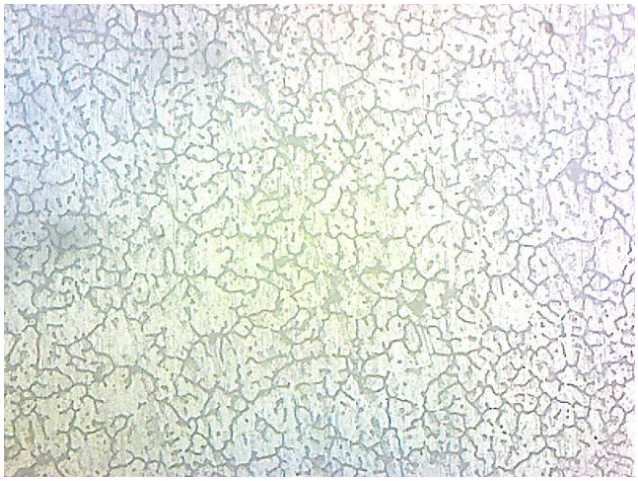

Weld bead

Figure 4.45: Microscopic images of optimized weld sample with ER5356 at X200

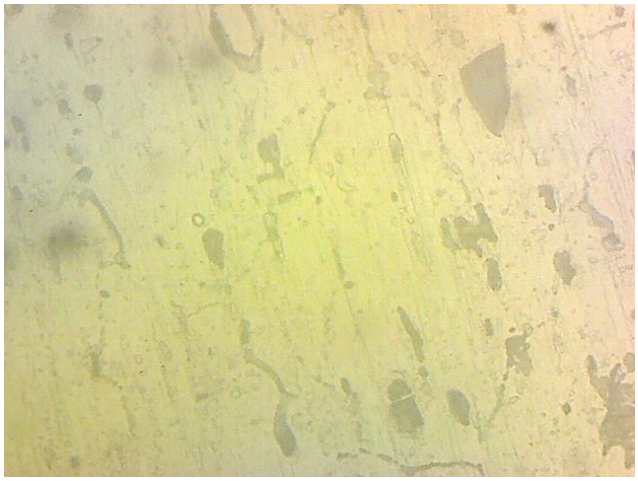

Base metal

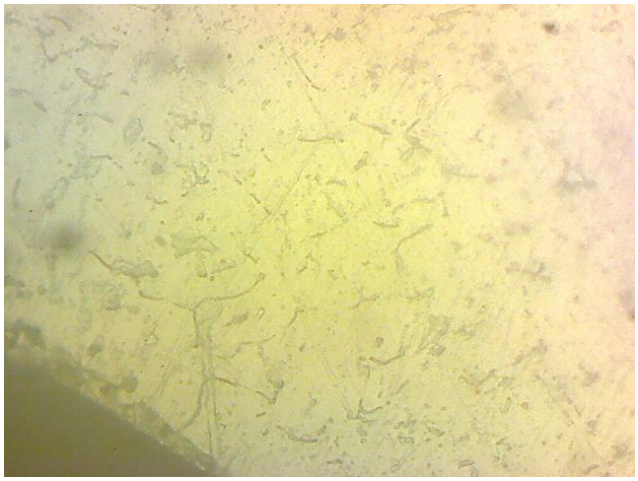

Heat affected area

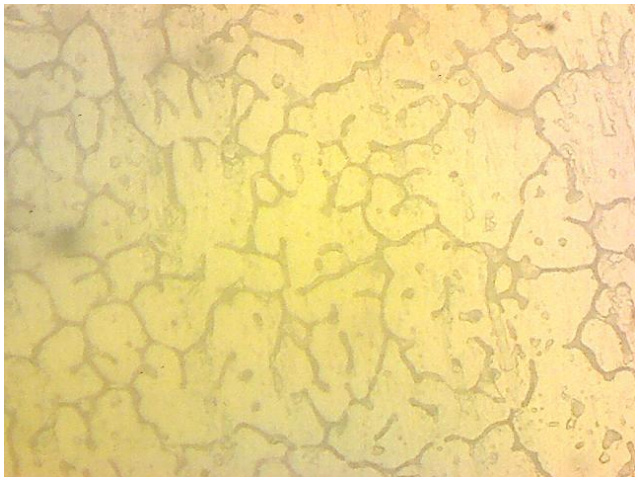

Weld bead

Figure 4.46: Microscopic images of optimized weld sample with ER5356 at X500

Above images shows the microstructure of TIG welded specimen of AA6082 with three different filler materials. In all the welded specimen's presence of overabundance of Mg_2Si can

be seen in parent metal AA6082 alloy. he darkish microstructure of the base metal reveals insoluble (Fencer)$_3SiAl_2$ particles and abundant soluble Mg_2Si particles.

Above analysis of microscopic images revealed that in every weld specimen grain structure at weld bead is column and equiaxed. The weld region covers eutectics of Mg2Si in main dendritic aluminium solid solution, as well as adherent sludge particles.

Microscopic images also suggest that Many grains had a greater density of misalignments with system structure, as well as porosity and cracks which results in lower tensile strength in welded joint in comparison to base metal.

Microstructure images of weld specimen with filler 5356 indicates that its grain size is smaller in comparison to grain size of weld specimens with ER4043 and ER4047, this is also one of the reasons that weld specimen with filler wire ER5356 has highest tensile strength.

CHAPTER 5

CONCLUSIONS AND FUTURE SCOPE

5.1 CONCLUSION

Various combination of experiments was conducted at different levels of welding electric current, Diameter of filler rod, and flow rate of argon by using L9 Taguchi orthogonal array technique with each filler wire. Total 27 samples have been tested. The mechanical properties of welded joint of AA6082 alloy with filler wires ER4043, ER4047 and ER5356 have been analysed by performing tensile test, microhardness test, residual stress and microstructure analysis, from the above calculation and Experiments, we find that-

1) Taguchi method used to optimise process parameter that affects the tensile strength of AA6082 alloy joint with filler wires ER4043, ER4047 and ER5356.

2) The optimum level of process parameters for AA6082 welded joint with filler wire ER4043 comes out at current (170 A), diameter of filler road (2.4 mm) and gas flow rate of argon gas (10 lt/min).

3) The optimum level of process parameters for AA6082 welded joint with filler wire ER4047 comes out at current (150 A), diameter of filler road (3.2 mm) and gas flow rate of argon gas (10 lt/min).

4) The optimum level of process parameters for AA6082 welded joint with filler wire ER5356 comes out at current (170 A), diameter of filler road (2.4 mm) and gas flow rate of argon gas (10 lt/min).

5) Maximum tensile strength of the joint with filler wire ER5356 is 187 MPa which is more than weld specimens with filler wire ER4043 which yield 179 MPa and ER4047 yields 181MPa.

6) Hardness value of weld specimen with ER5356 is also higher in comparison to its counter parts ER4043 and ER4047.

7) The value of residual stress of weld specimen with filler wire ER5356 is less in comparison to weld specimens with ER4043 and ER4047, due to weld specimen ER5356 is having highest tensile strength.

8) Welded specimen with filler wire ER5356 produces finer grains size in comparison to weld sepecimen with ER4043 and ER4047.

5.2 FUTURE SCOPE

There is a wide scope of research which can be explored in welding of AA6082 Aluminium alloy with different filler materials like:

1) During welding, problem of distortion is seen widely. It can be studied further to reduce it.
2) Effect of preheating and post heating need to be investigated for the best quality of joint.

REFERENCES

1. Luijendijk, T., "Welding of dissimilar aluminium alloys", International journal of Materials Processing Technology, vol. 103, pp.29-35, 2000

2. Missori, S. & Sili, A., "Mechanical behaviour of 6082-T6 aluminium alloy welds", J. Metallurgical Science and Technology, vol. 18, no. 1, pp.12-18, 2000.

3. Ambriz, Ricardo & Barrera Cardiel, Gerardo & García, Rafael & López. "A comparative study of the mechanical properties of 6061-T6 GMA welds obtained by the indirect electric arc (IEA) and the modified indirect electric arc (MIEA)", Materials & Design, vol. 30, pp.2446-2453, 2009.

4. Lakshminarayanan, A. K., Balasubramanian, V. & Elangovan, K., "Effect of welding processes on tensile properties of AA6061 aluminium alloy joints", Int. J. Adv. Manuf. Technol, vol. 40, pp. 286-296, 2009.

5. Wang, Q., Sun, D., Na, Y., Zhou, Y., Han, X. & Wang, J., "Effects of TIG Welding Parameters on Morphology and Mechanical Properties of Welded Joint of Ni-base Superalloy", Procedia Engineering, vol.10, pp. 37-41, 2011.

6. Norman, A. F., Drazhner, V. & Prangnell, P. B. "Effect of welding parameters on the solidification microstructure of autogenous TIG welds in an Al– Cu–Mg–Mn alloy", Materials Science and Engineering: A, vol.259, no.1, pp. 53-64, 1999.

7. Urena, A., Escalera, M. D. & Gil, L., "Influence of interface reactions on fracture mechanisms in TIG arc-welded aluminium matrix composites". Composites Science and Technology, vol.60, no.4, pp. 613-622, 2000.

8. Kumar, A. & Sundarrajan, S., "Optimization of pulsed TIG welding process parameters on mechanical properties of AA 5456 Aluminium alloy weldments". Materials & Design, vol. 30, no.4, pp.1288-1297, 2009.

9. Durgutlu, A., "Experimental investigation of the effect of hydrogen in argon as a shielding gas on TIG welding of austenitic stainless steel". Materials & design, vol.25, no.1, pp. 19-23,2004.

10. Hussain, A. K., Lateef, A., Javed, M. & Pramesh T., "Influence of Welding Speed on Tensile Strength of Welded Joint in TIG Welding Process". International Journal of Applied Engineering Research, Dindigul, vol.1, no.3, pp. 518-527, 2010.

11. Qinglei, J., Yajiang, L., Puchkov, U. A., Juan, W. & Chunzhi, X., "Microstructure characteristics in TIG welded joint of Mo–Cu composite and 18-8 stainless steel". International Journal of Refractory Metals and Hard Materials, vol. 28, no.3, pp.429-433, 2010.

12. Kumar, S., "Experimental investigation on pulsed TIG welding of aluminium plate", Advanced Engineering Technology, vol.1, no.2, pp. 200-211, 2010.

13. Indira Rani, M. & Marpu, R. N., "Effect of Pulsed Current Tig Welding Parameters on Mechanical Properties of J-Joint Strength of Aa6351", The International Journal of Engineering and Science (IJES), vol.1, no.1, pp. 1-5, 2012

14. Ghazvinloo, H. R., Honarbakhsh-Raouf, A., Shadfar, N., "Effect of arc voltage, welding current and welding speed on fatigue life, impact energy and bead penetration of AA6061 joints produced by robotic MIG welding". Indian J. of Science and Technology, vol.3, no. 2, pp.156-162, 2010

15. Mosneaga, V. A., Mizutani, T., Kobayashi, T. & Toda, H., "Impact Toughness of Weldments in Al–Mg–Si Alloys", Materials Transactions, vol. 43, pp.1381-1389, 2002.

16. Li, D., Lu, S., Dong, W., Li, D., & Li, Y., "Study of the law between the weld pool shape variations with the welding parameters under two TIG processes", Journal of Materials Processing Technology, vol. 212, no.1, pp.128-136, 2012

17. Karunakaran, N. "Effect of Pulsed Current on Temperature Distribution, Weld Bead Profiles and Characteristics of GTA Welded Stainless Steel Joints", International Journal of Engineering and Technology, vol.2, no.12, 2012

18. S. Juang. "Process parameter selection for optimizing the weld pool geometry in the tungsten inert gas welding of stainless steel", Journal of Materials Processing Technology, vol. 122, pp. 33-37, 2002

19. Shahi, Singh, S. S., Singla, N., Pandey, S. & Nanda, T., "Prediction of UTS And Toughness Properties of SAW Welded Joints", Proceedings of the Symposium of Joining of Materials, SOJOM, WRI, WMB-1, pp. 1-12, 2004

20. Pan, L. K., Wang, C. C., Hsiao, Y. C., and Hod, K. C., "Optimization of Nd: YAG laser welding onto magnesium alloy via Taguchi analysis", Optics Laser Technol., vol.37, pp.33-42, 2004.

21. Kumar, T. S., Balasubramanian, V. & Sanavullah, M. Y., "Influences of pulsed current tungsten inert gas welding parameters on the tensile properties of AA 6061 aluminium alloy", Materials and Design, vol. 28, pp.2080-2092, 2007.

22. Solic, S. & Busic, M., "The Influence of shielding gas on GTAW welding of aluminium thin sheets", International symposium on Electrical, Electronics and information engineering, pp. 335-338, 2021

23. Qiang Z., Han, Y., Jiquan, Z., Miao, L. & Xiaoguang, H., "Experimental study on Tig welding properties of 6061 and 7003 aluminium Alloys. IOP Conference Series: Earth and Environmental Science, pp.1755-1315,2021.

24. Kumar, G., Mohan, R., Dinesh, S., Prabhu, P. & Parthipan, N., "Investigation of the TIG Welding Process for Joining AA6082 Alloy Using Grey Relational Analysis", Advances in Materials Science and Engineering, vol.2022, pp.8,2022